minerals

MDPI

Article

Technologically Sustainable Route for Metals Valorization from Jarosite-PbAg Sludge

Željko Kamberović [1], Nataša Gajić [2,*], Marija Korać [1], Sanja Jevtić [1], Miroslav Sokić [3] and Jovica Stojanović [3]

[1] Faculty of Technology and Metallurgy, University of Belgrade, Karnegijeva 4, 11120 Belgrade, Serbia; kamber@tmf.bg.ac.rs (Ž.K.); marijakorac@tmf.bg.ac.rs (M.K.); sanja@tmf.bg.ac.rs (S.J.)
[2] Innovation Center of the Faculty of Technology and Metallurgy in Belgrade Ltd., University of Belgrade, Karnegijeva 4, 11120 Belgrade, Serbia
[3] Institute for Technology of Nuclear and Other Mineral Raw Materials, 11000 Belgrade, Serbia; m.sokic@itnms.ac.rs (M.S.); j.stojanovic@itnms.ac.rs (J.S.)
* Correspondence: ngajic@tmf.bg.ac.rs; Tel.: +381-605-236-021

Abstract: By-products from zinc hydrometallurgy are classified as hazardous waste with strong leaching toxicities. Even though numerous research papers are dedicated to valorizing valuable metals in it, the primary management route is still disposal or partial reuse, such as the Waelz process. Presented experimental research investigates possibilities of sulfidization and further processing as a technologically sustainable route for valuable metals valorization from non-standard jarosite-PbAg sludge. The comprehensive thermodynamic analysis was done by HSC Chemistry®, through optimizing process parameters, i.e., temperature, sulfur addition, and selection of possible additives. Technological possibility of magnetic separation, flotation, and smelting of sulfidized material was also investigated; the results were below the values that allow practical application, due to the obtained texture of sulfidized jarosite, which does not allow the liberation of minerals. Smelting tests were performed on sulfidized jarosite with sulfur and without and with carbon as additive. By smelting sulfidized jarosite-PbAg sludge with added carbon in sulfidization stage at 1375 °C, obtained products were matte, slag, raw lead, and dust in which base, critical, and slag forming components were valorized. Valuable metals were concentrated in smelting products so as to enable further processing, which also could be interesting in the case of treatment of complex, polymetallic, and refractory primary materials, which represent a significant contribution to the circular economy.

Keywords: jarosite-PbAg sludge; sulfidization; technological metals

Citation: Kamberović, Ž.; Gajić, N.; Korać, M.; Jevtić, S.; Sokić, M.; Stojanović, J. Technologically Sustainable Route for Metals Valorization from Jarosite-PbAg Sludge. *Minerals* **2021**, *11*, 255. https://doi.org/10.3390/min11030255

Academic Editor: Konstantinos Komnitsas

Received: 5 December 2020
Accepted: 24 February 2021
Published: 28 February 2021

1. Introduction

Total zinc mine production in 2019 was close to 13 million tons [1], mainly produced by roast-leach-electrowinning (RLE) processes. The leaching of calcine produces a pregnant solution containing high quantities of iron and various impurities, which are removed in the form of precipitate jarosite, goethite, or hematite. Precipitate forming processes, developed in the 1960s, no matter how advanced at the time, are the death knell for zinc pyrometallurgy and "The Iron Elephant", as stated by A.J. Monhemius in [2]. Every year around 6–7 million tons of these solid wastes are generated containing a variety of metals, whose disposal requires a very high standard of landfilling and monitoring, on top of the vast quantities already disposed of [3].

Jarosite formation is not only a problem in the zinc industry but also in other hydrometallurgical processes involving leaching and bioleaching of ores [4]. In addition, jarosite may precipitate during generation of acid mine drainage [5].

Jarosite waste is classified as hazardous waste [6] with strong leaching toxicity, metal mobility as well as significant biohazards [7], and the presence of toxic elements (As, Cd, Hg) and has an adverse impact on the environment. On the other hand, jarosite-PbAg

sludge contains significant amounts of the base (Zn, Pb, Cu, Fe), critical (In, Ga, Ge, Sb), and precious metals (Ag, Au) that could and should be recovered.

For the processing of jarosite sludge, several routes are proposed and investigated in scientific literature, such as stabilization for safer disposal or usage in civil engineering and hydrometallurgical and pyrometallurgical processing to recover contained valuable metals.

Stabilization is not a favorable option because contained metals are not recovered, and it could also be costly due to the used stabilizing agents, binders, and additives. However, more significantly, disposal is a pure loss of contained valuable metals because it prevents further treatment.

An old-fashion hydrometallurgical option is sulfatization and leaching, and one of the promising possibilities for treating side-streams from zinc- and steel-making plants is the Jarogain-process [8]. This very complex process generates almost 70% of waste compared to the input materials, which should be sent to the landfill/tailings dam or additionally treated as toxic waste.

Different pyrometallurgical plants, which are in operation in China, South Korea, India, Europe, and Australia utilizing Ausmelt furnace, Wealz kiln, or Pb Smelter/ISF + fumer, present more or less feasible routes with industrial confirmation [3,9,10]. For all of them, the common objective is that valuable metals, including Zn, Pb, Ag, In, and Cd, are recovered to a fume product and produce different and usually non-stable slags.

For the ArcFume process for direct smelting of combined residues (Jarosite and sulfur residue), despite showing good recovery of volatile metals such as Zn, Pb, Ag, In, and Ge, partial utilization on Cu, Ag, rare earth elements (REE) was achieved [11]. Application of electric furnaces for metal recovery is increased, adverse impact and energy consumption are decreased, and, by using lead as a metal collector, the utilization of valuable components is possible, thus smelting in the electric furnace could become a viable option [12]. The outdated Wealz process is still considered to be the best available technique and treats about one-third of all zinc-bearing residues, but it is necessary to add additives such as MgO to form environmentally stable slag [13]. During this process, the distribution of valuable components is unfavorable.

There are laboratory attempts on the recovery of the residual iron content within jarosite sludges through an Arc Transferred Plasma (ATP) and production of cast iron and glassy inert slag [14]. Obtained slag is in accordance with the idea of the investigated process, but produced white cast iron (high content of S, P, and Cu) can be used only as a small part of the charge, only if the charge is composed of Cu-free raw materials, which is hardly applicable.

Emerging techniques report chlorination in the rotary furnace and metalothermic process as a promising option. Even though authors state that, under optimized chlorination conditions, high volatilization rates of Zn, Pb, Cu, In, and Ag [15], the presence of high concentrations of chlorine in off-gasses is very corrosive and leads to frequent equipment maintenance. On the contrary, metallothemic shows promising results when a mixture of secondary Al and Mg is used as a reducing agent; at 1200 °C, the majority of Zn and Pb are vaporized [16].

As an alternative pyrometallurgical treatment, sulfidization could be used, which gained increasing attention as a potential approach for converting metal oxides to sulfides, which has good flotability and can be concentrated by the conventional flotation process.

A number of hydrometallurgical, mechanochemical, and pyrometallurgical sulfidization processes for recovering valuable metals from wastes have been investigated. This could be interesting in the case of complex, polymetallic, and refractory primary materials, especially in technogenic raw materials and urban e-wastes, where scientific efforts rely on synergy and incorporation in already existing materials flows. A summary of previous studies of sulfidization is presented in Table 1, mostly performed on synthetic systems.

Table 1. Summary of reviewed previous studies (p.a., pro analysis; n.a., not applicable).

Input Materials	T (°C)/t (h)	Sulfidization Efficiency	Flotation Efficiency	Overall Process Efficiency	Reference
Mechanical Ball Milling					
ZnO, p.a. + Al + S		96.70% Zn		25.00%	[17]
Hydrothermal Synthesis					
Zn-Pb ore + S	180 °C/4 h	73.00% Zn 86.00% Pb	92.00% Zn 93.00% Pb	67.89% Zn 79.98% Pb	[18]
Neutralization sludge + S	180 °C/2 h	85.00% Zn 75.40% Pb	33.30% Zn 58.96% Pb	28.31% Zn 44.46% Pb	[19]
Sulfidization Roasting					
Low grade Pb-Zn ore + S	650 °C/2 h	>98.00% Zn >95.00% Pb	89.90% Zn 83.68% Pb	88.20% Zn 79.50% Pb	[20]
PbZn carbonate + S	roasting 450 °C/1 h hold 750 °C/30 min	97.29% Zn 96.50% Pb	n.a.	n.a.	[21]
Lead smelter slag + S + Na_2CO_3	1000–1100 °C	91.25% Zn	75.64% Zn	88.34% Zn	[22,23]
Lead smelter slag + FeS_2 + Na_2CO_3	850 °C/2 h	>85.00% Zn	63.83% Zn 17.66% Pb	80.87% Zn	[24,25]
Jarosite + C	800 °C/2 h	98.00% Zn	n.a.	n.a.	[26]
ZnO p.a. + Na_2CO_3 + FeS_2 +C	850 °C	94.38% Zn	n.a.	*Increased*	[27]
ZnO p.a.+ S + Fe_2O_3 + C	1100 °C	97.50% Zn	n.a.	n.a.	[28]
Zn leaching residue	700–750 °C/1 h	85.00% decomposition rate of $ZnFe_2O_4$	n.a.	*Slight decrease*	[29]
Synthetic $ZnFe_2O_4$ + FeS_2	950 °C/1 h	83.12% Zn	*Authors claim that Zn and Fe could be recovered by the combined process of flotation-magnetic separation*		[30]
Blast furnace residue + S	850 °C/1 h	92.01% Zn	n.a.	n.a.	[31]
$PbSO_4$ p.a. + C	700 °C/1 h	86.45% Pb	87.12% Pb	75.32% Pb	[32]

The results presented in Table 1 indicated that temperature plays an important role in the sulfidization roasting process, especially in the formation and growth of ZnS crystals [20,21]. The increase of temperature promotes crystallization and growth of ZnS crystals, which is favorable for the flotation process, but resulted in accelerated volatilization of sulfur. The addition of 15% of carbon led to successfully performed sulfidization of jarosite waste by reduction roasting, achieving maximal efficiency of 98% [26].

Reduction roasting followed by magnetic separation has been proposed to separate iron, leaving a non-magnetic product enriched in zinc and lead and more suitable for a sulfidization [33]. Wang and coworkers [34,35] investigated the recovery of valuable metals: lead, zinc, and iron, from jarosite residues, using magnetic-milling separation after reduction roasting, simultaneously fixing the hazardous element sulfur in the roasting product. The grade of the resulting magnetic fraction was 90.59% Fe with an iron recovery of 50.87%. In another investigation [36], it was shown that the pelletizing process is more suitable for recovering valuable metals from jarosite residues through direct reduction. The decomposition of zinc ferrite into ZnO and Fe_3O_4 using a mixture of CO and Ar gas as reducing agents were investigated [37]. Low temperature (460 °C) magnetization using reducing gas, led to full conversion of Goethite and jarosite into magnetite through solid-

state transformation [38], and recovery of 93.00% of the magnetite by magnetic separation. Similarly, the gas-based fluidized magnetization roasting was done in [39], where most of the hematite and siderite particles were converted to magnetite successfully.

To promote the sulfidization rate, optimize grain morphology, and thereafter improve flotability, further knowledge of the sulfidization reactions is necessary. In this paper, the process of sulfidization of non-standard jarosite-PbAg sludge was investigated for the valorization of useful components. Process thermodynamics at different temperatures and in the presence of various additives were analyzed using HSC Chemistry® 9.9.2.3. Additionally, the potential application of magnetic separation, flotation, and smelting for the valorization of sulfidized material was explored. Summary of conclusions from literature review could be expressed in one sentence: refractoriness of jarosite-PbAg sludge is related to its generic origin, complex chemical composition and morphology, and the inability to liberate valuable components without a complete transformation of the primary matrix. Literature results, based on pure systems, are not useful for understanding the phenomena in real systems, especially due to the number of impurities that fundamentally change process mechanism. The experimental research's primary goal was obtaining results for maximal technologically possible utilization of metals and formation of stable products.

2. Experimental

2.1. Materials

The jarosite-PbAg sludge generated from Serbian primary zinc production had been deposited in open tailing dams within the industrial area. The tailing dam has a surface area of approximately 60,000 m^2, and the various waste materials were disposed of at this location for more than 50 years. The 354 holes with a total depth of approximately 2000 m were drilled in the tailings from which 3294 samples were collected, homogenized, and formed the representative sample. The sample was dried at 105 °C and stored in polyethylene containers. The dried jarosite-PbAg sludge was ball milled for 1 h for deagglomeration. The bulk density of the final sample (after drying and milling) was 0.77 $g \cdot cm^{-3}$. As prepared, samples were sieved to −100 μm for analysis and experiments.

The commercially available sulfur powder (purity 99.90%, bulk density 0.59 $g \cdot cm^{-3}$, Solvay & CPC, Hannover, Germany) was used as sulfidizing agent. Lead(II)−oxide (purity 99.70%, Acros Organic, Fair Lawn, NJ, USA), sodium carbonate (Betahem, Serbia), bornite, and commercial graphite (powder with particle size < 64 μm, purity 95.00%) as additives were used in the experiments. Nitrogen with 99.99% purity was used as the protective gas for creating an inert atmosphere during the sulfidization process. In order to investigate the behavior of selected phases during sulfidization of jarosite-PbAg sludge, zinc ferrite ($ZnFe_2O_4$) was synthesized using zinc chloride ($ZnCl_2$, p.a., Acros Organics) and iron(III) chloride hexahydrate ($FeCl_3 \cdot 6H_2O$, p.a. Sigma-Aldrich, St. Louis, MO, USA) according to the procedure described in [40].

2.2. Sulfidization of the Jarosite-PbAg Sludge and Zinc Ferrite

The sulfidization process of jarosite-PbAg sludge was carried out in a rotary tilting tube furnace (ST-1200RGV, Zhengzhou, China). The jarosite-PbAg sludge and sulfur powder with and without additives were mixed for 15 min in the mixer. The quantity of additives Na_2CO_3, Cu_5FeS_4, and PbO was 10.00 wt.%, and the quantity of C was in the range 2.00–10.00 wt.% of the mixture. Then, the as-prepared homogenized mixture was transferred to a covered ceramic boat. The boat was placed in the center of the quartz tube and into the furnace. High-purity nitrogen gas was introduced through one side of the furnace, while the other side of the quartz tube was connected to a cooling system and outlet gas washing system. The total flow rate of the N_2 gas was fixed at 5 $dm^3 \cdot h^{-1}$ for all experimental conditions. Before heating the furnace, nitrogen gas was continuously flushed for about 10 min to remove residual air from the furnace. The sulfidization of jarosite-PbAg sludge was performed in five temperature stages 135, 260, 360, 460, and 550 °C. To prolong the contact time of sulfur and jarosite-PbAg sludge in the starting

powder mixture, before sulfur evaporation, which promotes the transformation of sulfur to a gas phase and the loss of a large amount of S and/or SO_2, samples maintained under these conditions for 30 min; further sulfidization process was carried out at 900 °C for 30 min. Additionally, in order to improve contact between jarosite-PbAg sludge and sulfur powder a part of prepared mixtures was pressed using laboratory press with pressing force of 500 KN. Then as-prepared samples were treated in the furnace. Figure 1 shows a flowsheet of the experimental process. Sulfidization of $ZnFe_2O_4$ was performed in same manner as sulfidization of jarosite-PbAg sludge.

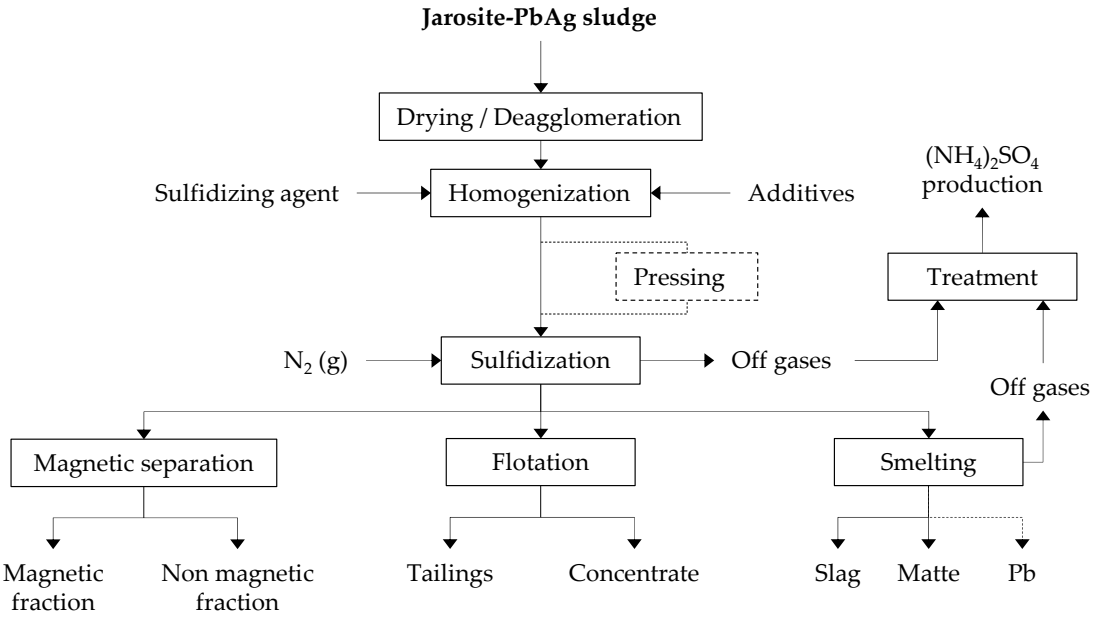

Figure 1. The flowsheet of experimental process.

2.3. Magnetic Separation

Laboratory investigation of magnetic separation was performed on ground samples −37 μm in the drum permanent magnet separator, SALA, by the wet method, magnetic field strength 700 G.

2.4. Flotation Procedure

Sulfidized samples for collective flotation concentration were grounded to −63 μm, and samples for Pb + Zn concentrate were grounded to −37 μm using a ball mill.

Sodium cyanide and $ZnSO_4$ as a depressant, $CuSO_4$ as an activator, methyl-terminated polypropylene glycols (KAX) as a collector, and methyl-terminated polypropylene glycols (D250) as a frother were used in the flotation process. All of these agents for flotation are of analytical grade. The flotation was carried out at pH = 9 and with a stirring rate of 1000 min^{-1}.

2.5. Smelting Tests

The first series of tests were performed to investigate the possibility of processing jarosite-PbAg sludge as received utilizing a submerged DC plasma process, using a semi-industrial DC arc-furnace, the power of 100 KW a 0.40 m^3 working capacity, with a combined refractory lining, ordered from inside to outside: high-magnesite, sinter magnesite, and corundum, equipped with an off-gas cooling system and bag filter. The test was performed by processing 30.0 kg of input material, using a synthesized FCS (ferrous calcium silicates) as a starting slag system (~10.00 wt.% of charge). The starting slag was produced by melting a dry homogenized mixture of FeO, CaO, and quartz sand (SiO_2) in ratio Fe/SiO_2 = 1 and CaO 12.50%. After melting, the material was cast into a cru-

cible and cooled on air. The casting temperature, 1325–1375 °C, was measured using an immersion pyrometer.

Smelting process aimed at the recovery of zinc, lead, silver, indium, and germanium in filter product. Copper present in the raw material should be recovered as a metal, together with nickel and cobalt, and the resulting slag should be leach stable. The process started with melting the starting slag. After melting the starting slag jarosite mix (jarosite-PbAg sludge + 10.00% coke + 10.00% lime) was charged. Separation of the physical matte droplets by gravitation from the slag was finalized only in the slag pots during the initial solidification. Basicity of slag was calculated as the ratio between CaO + MgO and SiO_2 + Al_2O_3.

Smelting of sulfidized jarosite was performed in the same manner but without the addition of coke and lime in the furnace. Anticipated products were matte, slag, raw lead, and dust.

Prior to smelting in a submerged DC arc furnace, two sets of experiments were performed on sulfidized jarosite-PbAg sludge in a chamber furnace (ST-1600MX-III) with the addition of 10.00% of $Li_2B_4O_7$. The samples were placed into the preheated SiC crucible, and then the crucible was placed again in the furnace for 1 h at 1375 °C. After cooling, the sample has been removed from the crucible.

All experiments were performed in triplicate.

2.6. Methods

The phase composition of jarosite-PbAg sludge was determined by X-ray diffraction analyses using an Ital Structure diffractometer (APD2000) with CuKα radiation (λ = 1.54 Å). Measurements were carried out in the 2θ range from 5° to 65° in steps of 0.02. The chemical composition of the samples was determined by combining different instrumental methods: inductively coupled plasma-atomic emission spectroscopy (ICP-MS), X-ray fluorescence (XRF), atomic absorption spectroscopy (AAS), infrared absorption on the LECO CS230 analyzer, and inductively coupled mass spectroscopy (IMS) (SGS methods, codes: ICP40Q, ME-MS61, AAS43B, CSA06V, IMS40Q). The total sulfur in the jarosite-PbAg sludge sample was determined using combustion techniques with a LECO CS230 instrument. The samples were analyzed for the presence of zinc and lead by using an atomic absorption spectrophotometer PE 4000. The concentration of Fe, Ag, Al, Sb, Ti, and Cr were determinate using PE Plasma 400. A Smiths Detection Ionscan 400 was used for the determination of Ga, In, Na, Mn, Cu, As, K, Cd, Sn, and Bi. XRF analysis was carried out on the Vanta Olympus for elemental analysis of sulfidized and melted products.

Thermal analysis was performed using an SDT Q-600 simultaneous DSC-TGA instrument (TA Instruments). The samples were heated in a standard alumina sample pan from room temperature to 1000 °C at a heating rate of 10 °C min^{-1} under nitrogen with a flow rate of 0.10 $cm^3 \cdot min^{-1}$. The TG instrument was coupled to a Hiden HPR-20/QIC mass spectrometer (MS) for gas analysis. Water vapor, ammonia, and sulfur dioxide were analyzed. The analysis of FTIR spectra was used for the identification of functional groups of jarosite-PbAg sludge. Transmittance spectra were obtained using a Digilab-FTS 80 FTIR spectrometer and samples pressed into KBr pellets. Data were recorded from 4000 to 600 cm^{-1}. Carrier particle sizer was measured using a laser diffraction particle size analyzer (Sympatec, GmbH) consisting of a HELOS/KF laser diffraction sensor, a RODOS dry dispersing unit, and a VIBRI vibratory feeder.

The thermodynamics of jarosite-PbAg sludge sulfidization were investigated by HSC Chemistry® software package 9.9.2.3 [41].

The qualitative mineralogical analysis was performed under a polarizing microscope for the reflected light in the air and oil immersion, with the identification of phases in sulfidized samples. A JENAPOL-U polarizing microscope for reflected and transmitted light with a "Carl Zeiss AxioVision SE64 Rel. 4.9.1." software package equipped with a "Multiphase" module and an "Axiocam 105 color" camera was used for the mineralogical examinations.

3. Results and Discussion

3.1. Characterization of the Jarosite-PbAg Sludge and $ZnFe_2O_4$

The XRD pattern of jarosite-PbAg sludge is shown in Figure 2. The major phases are ammonium jarosite ($NH_4Fe_3(SO_4)_2(OH)_6$, JCPDS no. 96-901-1834), quartz (SiO_2, JCPDS no. 96-412-4049), anglesite ($PbSO_4$, JCPDS no. 96-154-2012), and zinc ferrite ($ZnFe_2O_4$, JCPDS no. 96-900-5103). Considering that the diffractions of potassium- and ammonium-jarosite are very close, TG-MS and FTIR analysis have confirmed that ammonium jarosite is present in the examined sample.

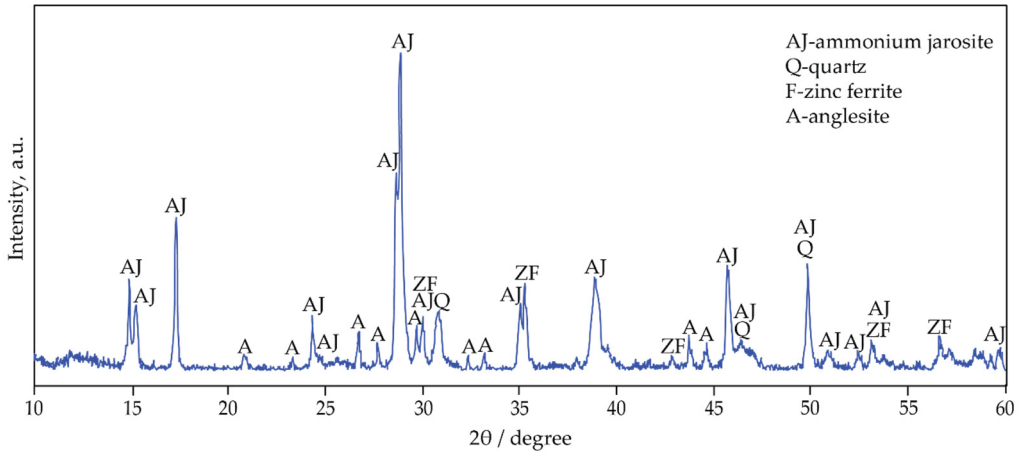

Figure 2. XRD pattern of jarosite-PbAg sludge.

In addition, to examine the behavior of pure zinc ferrite in the sulfidization process, it was determined according to the database ($ZnFe_2O_4$, JCPDS No. 96-900-5103) that pure zinc ferrite was synthesized and that the observed diffractions cannot be attributed to other compounds.

Elemental analysis was used to quantify the elements present in the jarosite-PbAg sludge sample (Table 2).

The results of the elemental analysis showed approximately 27 wt.% of iron, as well as 7 wt.% of lead, zinc, and sulfur, and also metals of interest such as silver, gallium, and indium in concentrations of 200, 100, and 200 ppm, respectively. About 6 wt.% of other metals (Ca, Al, Na, Mn, Cu, etc.) are present in the sample.

Figure 3 presents the thermogravimetric analysis of jarosite-PbAg sludge. The TG-DTG curves (Figure 3) show that the sample is thermally stable up to 250 °C, which confirms that all adsorbed moisture has been removed by the previous drying. In the temperature range, 250–1000 °C, the sample mass loss in three steps was detected. It is observed that the total weight loss is approximately 32 wt.%.

Table 2. Elemental analysis of jarosite-PbAg sludge.

Element	Concentration, wt.%	Method
Fe	27.25	ICP40Q
Pb	7.04	AAS43B
Zn	6.96	AAS43B
S	6.97	CSA06V
Ag	0.02	ICP40Q
Ga	0.01	IMS40Q
In	0.02	IMS40Q
Ca	1.57	ME-MS61
Al	1.06	ICP40Q
Na	0.94	IMS40Q
Mn	0.62	IMS40Q
Cu	0.52	IMS40Q
As	0.39	IMS40Q
K	0.13	IMS40Q
Sb	0.12	ICP40Q
Mg	0.10	ME-MS61
Ti	0.07	ICP40Q
Cd	0.06	IMS40Q
Sn	0.03	IMS40Q
Sr	0.02	IMS40Q
Bi	0.01	IMS40Q
Cr	0.01	ICP40Q

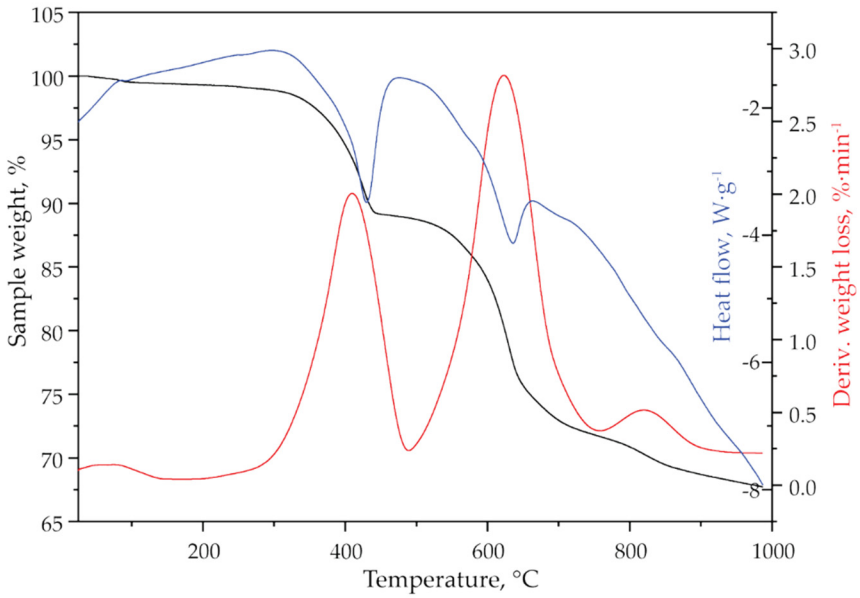

Figure 3. TG (black line), DTG (red line), and DSC (blue line) curves of jarosite-PbAg sludge.

First weight loss (11.00 wt.%) at temperature interval 250–490 °C with DTG maximum at 420 °C could be attributed to the loss of hydroxyl and ammonium groups. The presence of ammonia and hydroxyl units as H_2O in the gas phase obtained by decomposition of the sample was also confirmed by mass spectrometry (Figure 4, m/z 17 and 18) which is consistent with XRD analysis. The second weight loss (about 17 wt.%) occurs in the range of 490–750 °C (DTG maximum at 630 °C) and could be attributed to the loss of sulphur compounds as SO_2. The loss of sulfate is evidenced by the mass gain of SO_2 (m/z 64), as shown in Figure 4. Three distinct mass gains are observed at 564, 625, and 680 °C. The third mass loss (about 4 wt.%) occurs in the range of 750–900 °C with a DTG maximum at 845 °C. According to the literature, this weight loss could be attributed to the degradation of anglesite, $PbSO_4$ [42]. Mass gain at MS spectrum (Figure 4) observed at 830 °C can be

attributed to sulfur dioxide formed by the decomposition of $PbSO_4$. The DSC curve shown in Figure 3 indicates that the jarosite decomposition is an endothermic process.

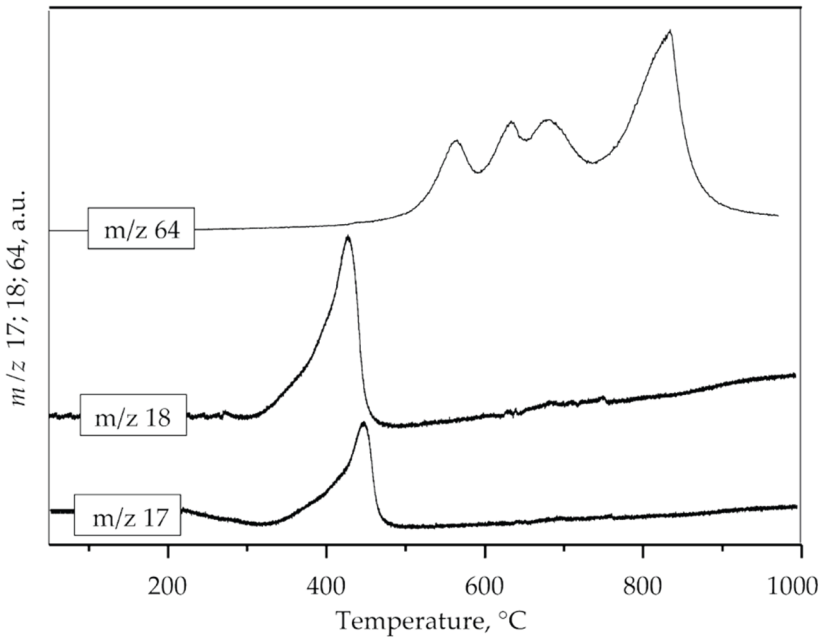

Figure 4. MS spectrum of ammonia (m/z 17), water (m/z 18) and sulfur dioxide (m/z 64).

Using the formula of ammonium jarosite as $(NH_4)Fe_3(SO_4)_2(OH)_6$, the theoretical mass losses for ammonia and hydroxyl units as H_2O are about 25 wt.%. Considering that the mass loss in the first step of thermal decomposition, which is attributed to the loss of water and ammonia, was 11.00 wt.%, it can be calculated that the sample contains 44.00 wt.% jarosite. Theoretically, expected weight loss due to SO_2 release for this amount of jarosite should be 17.60 wt.%. The obtained experimental data (17.00 wt.%), which is attributed to the SO_2 in the second step of mass loss (490–750 °C) showed good agreement with the theoretical assumptions.

Considering results of elemental and thermogravimetric analysis, phase composition of jarosite-PbAg sludge was determined (Table 3).

Jarosite-PbAg sludge was also studied using FTIR spectroscopy (Figure 5). The band at 3432 cm^{-1}, present in IR spectra, is related to the vibration of the hydroxyl groups. A band at 1634 cm^{-1} is associated with the deformation vibration of the absorbed water, whereas the band at 1426 cm^{-1} is assigned to an N-H bending mode in the NH_4^+ group [40]. The presence of the vibrations band corresponding to the ammonium group confirmed that ammonium jarosite was present in the sample. Three intense absorption bands at 1192, 1078, and 1001 cm^{-1} are assigned to sulfate species. Several absorptions were also observed in the 400 to 1000 cm^{-1} region. The absorption at 630 cm^{-1} can be attributed to the vibration mode of sulfate, whereas IR bands observed at 506 and 471 cm^{-1} correspond to vibrations of FeO_6 coordination octahedral units [43].

Table 3. The phase composition of the jarosite-PbAg sludge.

Phases	Content, wt.%
CaO	2.20
CuO	0.65
$NH_4Fe_3(SO_4)_2(OH)_6$	44.00
$ZnFe_2O_4$	25.70
K_2O	0.32
MgO	0.16
Na_2O	1.27
$PbSO_4$	10.30
SiO_2	11.50
TiO_2	0.11
Bi_2O_3	0.01
CdO	0.07
Cr_2O_3	0.02
In_2O_3	0.03
MnO	0.80
P_2O_5	0.09
Sb_2O_3	0.14
SnO_2	0.04
SrO	0.02
Al_2O_3	2.01
Ga_2O	0.02
AgO	0.02
As_2O_3	0.51
Total	100.00

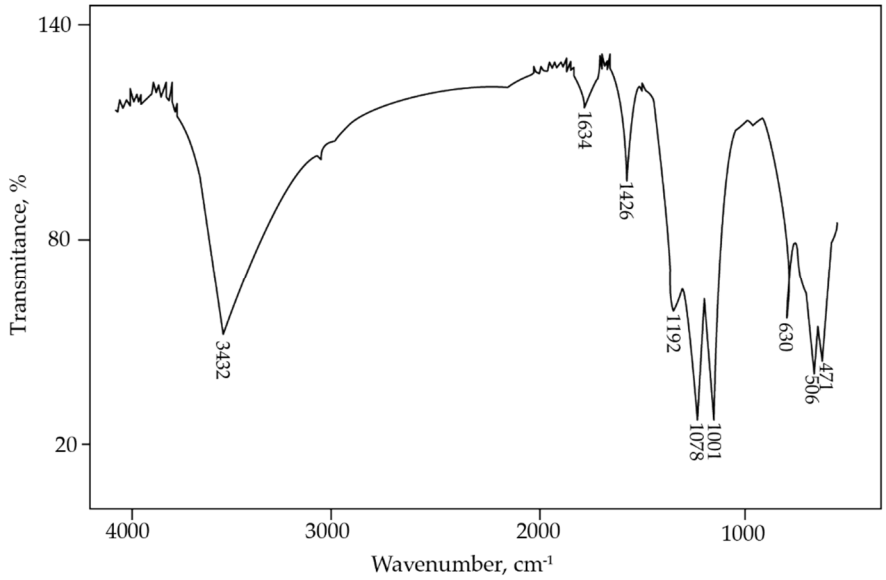

Figure 5. FTIR spectrum of jarosite-PbAg sludge.

Size distribution data of dried jarosite-PbAg sludge sample obtained from laser diffraction measurements are plotted as a particle and cumulative size distribution and shown in Figure 6. It is shown that the median diameter of particles is 1.58 μm.

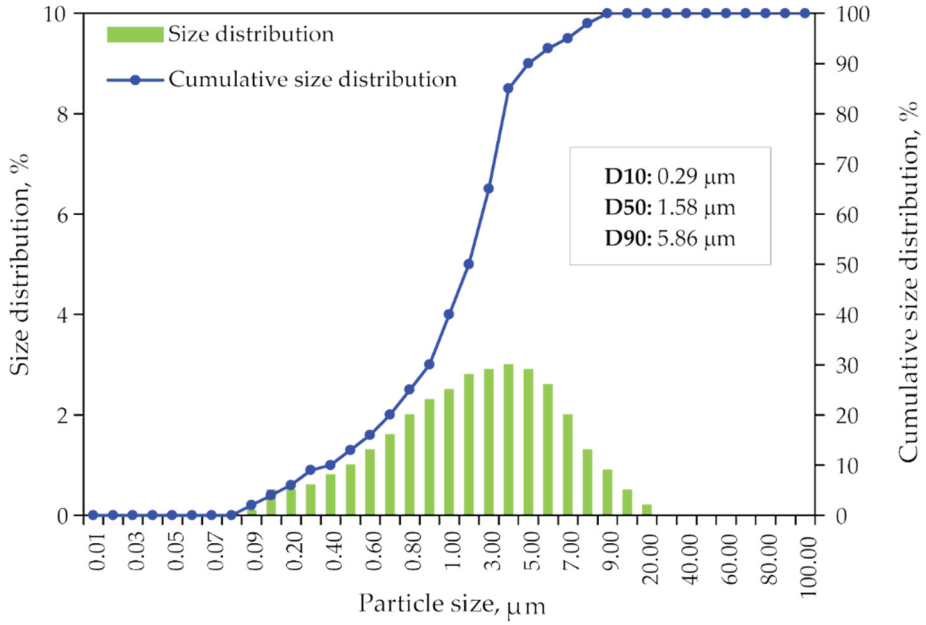

Figure 6. Particle size distribution and the cumulative size distribution of jarosite-PbAg sludge.

3.2. Thermodynamic Analysis

As any reliable thermodynamic data for ammonium jarosite were not available in HSC software, as start components for thermodynamic calculations, the main products of the thermal decomposition of ammonium jarosite: $Fe_2(SO_4)_3$, Fe_2O_3, $NH_3(g)$, and $H_2O(g)$ were used.

The results of the thermodynamic analysis of the sulfidization process are discussed below. According to the jarosite-PbAg sludge phases composition, with regards to the main constituents metals Equations (1)–(5), metals of interest Equations (6)–(8), and other metals Equations (7)–(23), the following chemical reactions were considered in the sulfidization process (Table 4).

Figure 7 shows plots of the standard Gibbs free energy (Δ_rG^θ) of reactions versus temperature for Equations (1)–(23) in the temperature range from room temperature up to 1000 °C.

Reactions presented with Equations (1)–(8) are theoretically possible from the thermodynamic point of view and proceed spontaneously at temperatures higher than 360 °C ($\Delta_rG^\theta < 0$), as shown in Figure 7a, and Table 4. In the case of reactions presented in Figure 7b, Equations (9)–(19), negative Δ_rG^θ values are obtained at temperatures around 500 °C. However, among them, the change of the Gibbs energy of reactions, presented with Equations (20)–(23), has a positive value over the entire temperature range, and these reactions will not occur spontaneously. Thermodynamically, the more negative the Δ_rG^θ value is, the easier it is for the reaction to occur. The formation of Ag and Ga sulfides (Equations (6) and (7)) occurs first, then at a higher value of Δ_rG^θ ZnS, FeS, and FeS_2 are formed from $ZnFe_2O_4$, as well as the corresponding oxides (Fe_2O_3 and Fe_3O_4). The reactions of the formed oxides (Fe_2O_3, Fe_3O_4) with the sulfidizing agent (S) take place simultaneously, whereby pyrite is formed, which also has the role of a reducing agent and forms ZnS in the reaction with $ZnFe_2O_4$. As can be seen from Figure 7b, indium sulfide is formed at temperatures higher than 200 °C, and PbS at temperatures higher than 360 °C. After the decomposition of jarosite and the formation of $Fe_2(SO_4)_3$, at temperatures above 389 °C, iron oxides (Fe_2O_3 and Fe_3O_4) and iron sulfides (FeS and FeS_2) are formed.

The Δ_rG^θ-T relationship suggests that the sulfidization of jarosite-PbAg sludge components thermodynamically can occur at a temperature around 550 °C, except for TiO_2, P_2O_5, MgO, and Cr_2O_3 phases.

Table 4. Reactions of jarosite-PbAg sludge with sulfur.

Group	Equations	No.
Main constituents metals	$3.5ZnFe_2O_4 + 10S = 3.5ZnS + FeS + Fe_2O_3 + Fe_3O_4 + FeS_2 + 3.5SO_2(g)$	(1)
	$3.5Fe_2(SO_4)_3 + 7.25S_2(g) = 2FeS + 19SO_2(g) + 2FeS_2 + Fe_3O_4$	(2)
	$4NH_3(g) + S_2(g) = 2H_2S(g) + 2N_2(g) + 4H_2(g)$	(3)
	$Fe_2O_3 + 1.75S_2(g) = 2FeS + 1.5SO_2(g)$	(4)
	$PbSO_4 + 2S = PbS + 2SO_2(g)$	(5)
Metals of interest	$2AgO + 2S = Ag_2S + SO_2(g)$	(6)
	$2Ga_2O + 7S = 2Ga_2S_3 + SO_2(g)$	(7)
	$In_2O_3 + 4.5S = In_2S_3 + 1.5SO_2(g)$	(8)
Other metals	$2CaO + 3S = 2CaS + SO_2(g)$	(9)
	$2Na_2O + 3S = 2Na_2S + SO_2(g)$	(10)
	$2MnO + 5S = 2MnS_2 + SO_2(g)$	(11)
	$3CuO + 3.5S = Cu_2S + 1.5SO_2(g) + CuS$	(12)
	$As_2O_3 + 4.5S = As_2S_3 + 1.5SO_2(g)$	(13)
	$2K_2O + 3S = 2K_2S + SO_2(g)$	(14)
	$2CdO + 3S = 2CdS + SO_2(g)$	(15)
	$Sb_2O_3 + 4.5S = Sb_2S_3 + 1.5SO_2(g)$	(16)
	$SnO_2 + 3S = SnS_2 + SO_2(g)$	(17)
	$Bi_2O_3 + 3.5S = 2BiS(g) + 1.5SO_2(g)$	(18)
	$2SrO + 3S = 2SrS + SO_2(g)$	(19)
	$TiO_2 + 3S = TiS_2 + SO_2(g)$	(20)
	$P_2O_5 + 7.5S = P_2S_5 + 2.5SO_2(g)$	(21)
	$2MgO + 3S = 2MgS + SO_2(g)$	(22)
	$Cr_2O_3 + 4.5S = Cr_2S_3 + 1.5SO_2(g)$	(23)

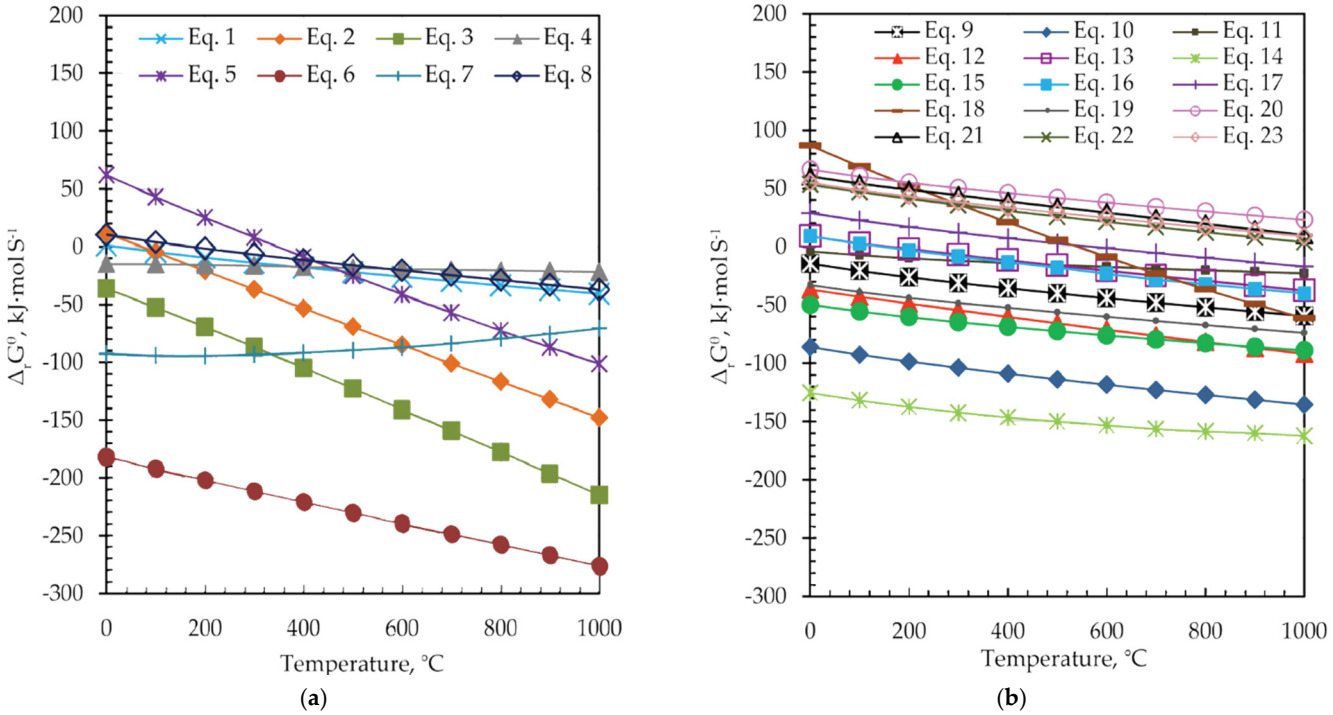

Figure 7. The change in standard Gibbs free energy (Δ_rG^θ) versus temperature for (**a**) Equations (1)–(8) and, (**b**) Equations (9)–(23).

3.2.1. Effects of Sulfur Addition

The effect of sulfur dosage on the equilibrium composition at 550 °C of the analyzed system is illustrated in Figure 8a–c. The equilibrium composition was calculated using

the HSC based on the Gibbs energy minimization method to examine the thermodynamic mechanism of the sulfidization of jarosite-PbAg sludge. The calculations were performed on 100.00 kg of jarosite-PbAg sludge under the pressure of 1.00 atm.

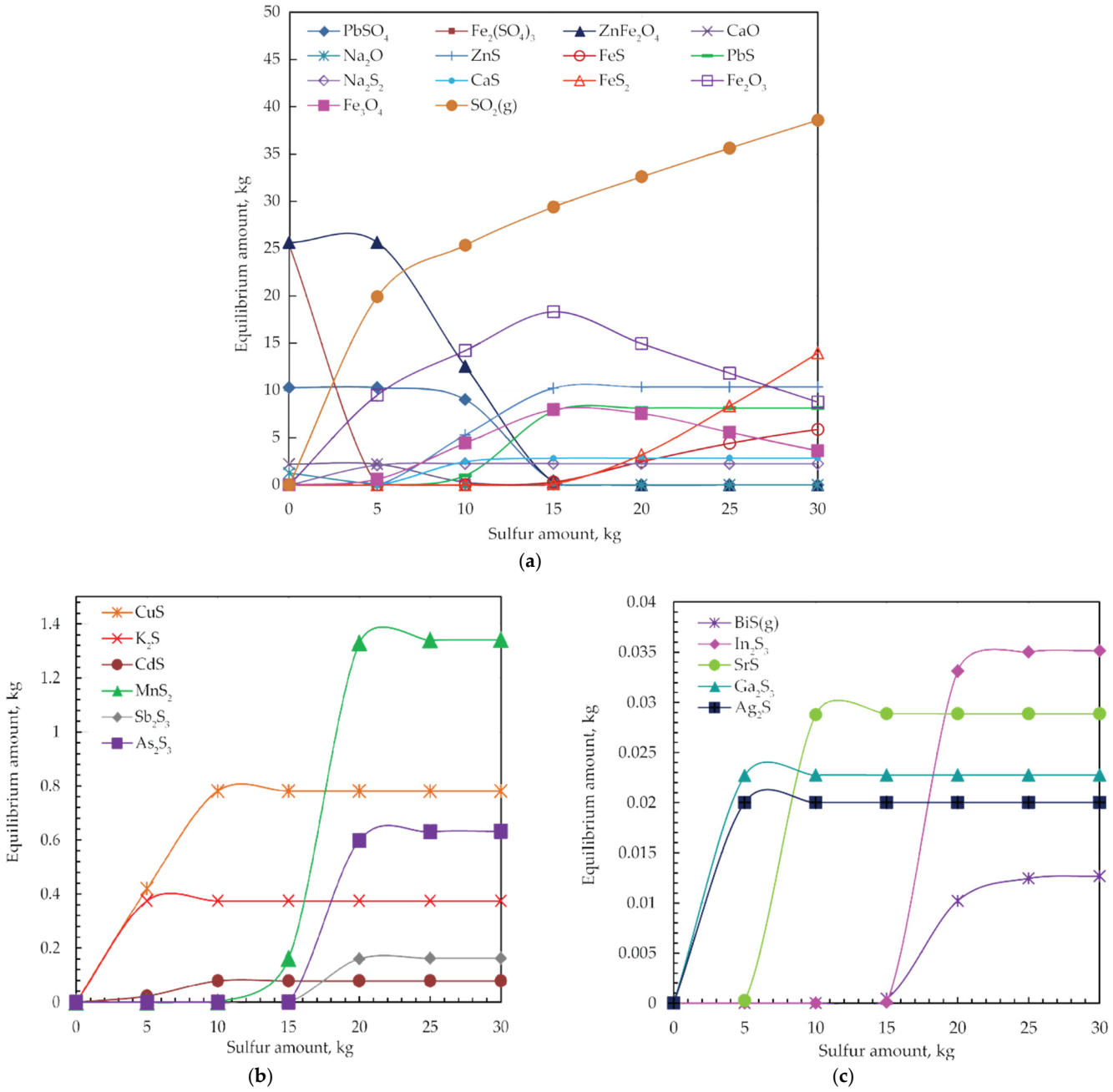

Figure 8. Equilibrium phase diagrams of (**a**) main and (**b**,**c**) minor products of jarosite-PbAg sludge reaction with different sulfur amounts at 550 °C.

When 5.00 kg of sulfur is added, Zn sulfide begins to form and reaches a maximum amount by adding 15.00 kg of sulfur, when ferrite is completely consumed. With the further addition of sulfur, the amount of ZnS remains constant. Lead sulfide starts to form when 8.00 kg sulfur is added, and its amount is maximal when 15.00 kg of sulfur is added, and, after that, its amount is constant. Sodium sulfide starts to form immediately with the addition of sulfur, and, with 5.00 kg·S, the addition reaches its maximum amount when Na_2O is completely consumed. As the sulfur dosage reaches 5 kg sulfides of calcium appear, and their contents increase and remain constant with a sulfur dosage of 10.00 kg.

The contents of iron oxides (Fe_2O_3 and Fe_3O_4) gradually increase with the increase in sulfur dosage, whereas the content of the $Fe_2(SO_4)_3$ decreases gradually. Also noted, at 15.00 kg sulfur dosage, iron sulfide phases (FeS and FeS_2) appear, and its content increases with the increase in sulfur dosage. In order to suppress the formation of iron sulfides in favor of iron oxides formation, the sulfur dosage must not be more than 15.00 kg. The thermodynamic analysis suggests the appearance of the magnetite phase.

At the point of 15.00 kg of sulfur dosage, the entire amounts of main components of jarosite-PbAg sludge are consumed, and Zn and Pb sulfides predominate phases.

However, as shown in Figure 8b,c, it can be seen that the stability of other sulfides was achieved by adding 20.00 kg of sulfur. With a further increase in sulfur dosage, the amount of sulfides kept a constant value.

The contents of Ag, Ga, and In sulfides gradually increase with the increase in sulfur dosage, until 1.00, 5.00, and 20.00 kg, respectively, after which they remain constant.

The temperature effect and addition of sulfur on phases produced were investigated thermodynamically to determine optimal parameters for various routes to treat jarosite-PbAg sludge (Figure 9).

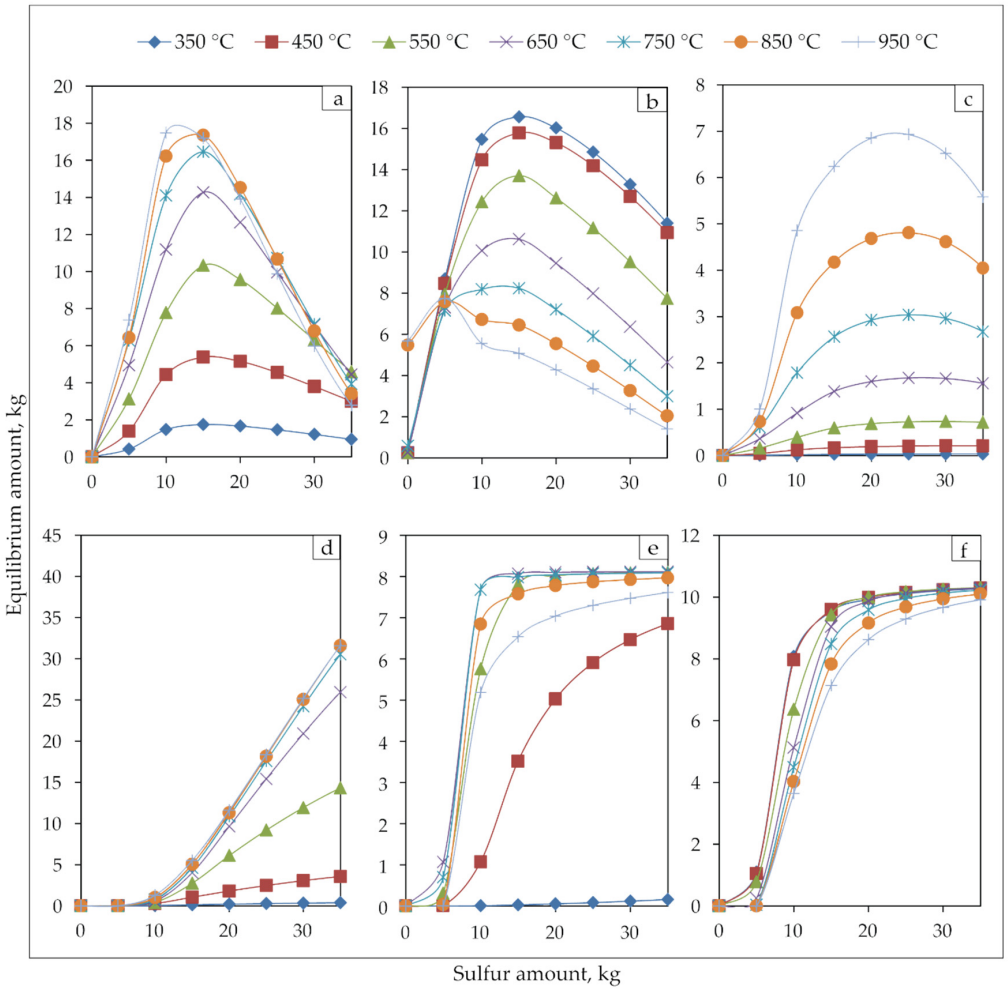

Figure 9. Equilibrium phase diagrams of (**a**) Fe_3O_4, (**b**) Fe_2O_3, (**c**) FeO, (**d**) FeS, (**e**) PbS, and (**f**) ZnS during jarosite-PbAg sludge with different sulfur amount at 350, 450, 550, 650, 750, 850 and 950 °C.

The amounts of all phases gradually increase at all temperatures until the addition of the sulfur is around 15 kg. With the further addition of sulfur, the Fe_3O_4, Fe_2O_3, and FeO phases begin to decrease significantly, the amount of FeS continues to increase, and PbS and ZnS phases remain constant.

3.2.2. Effect of Additives

Figure 10 shows the effect of different additives (Na_2CO_3, Cu_5FeS_4, PbO, and C) up to 15% at a temperature of 550 °C on the sulphidation jarosite-PbAg sludge.

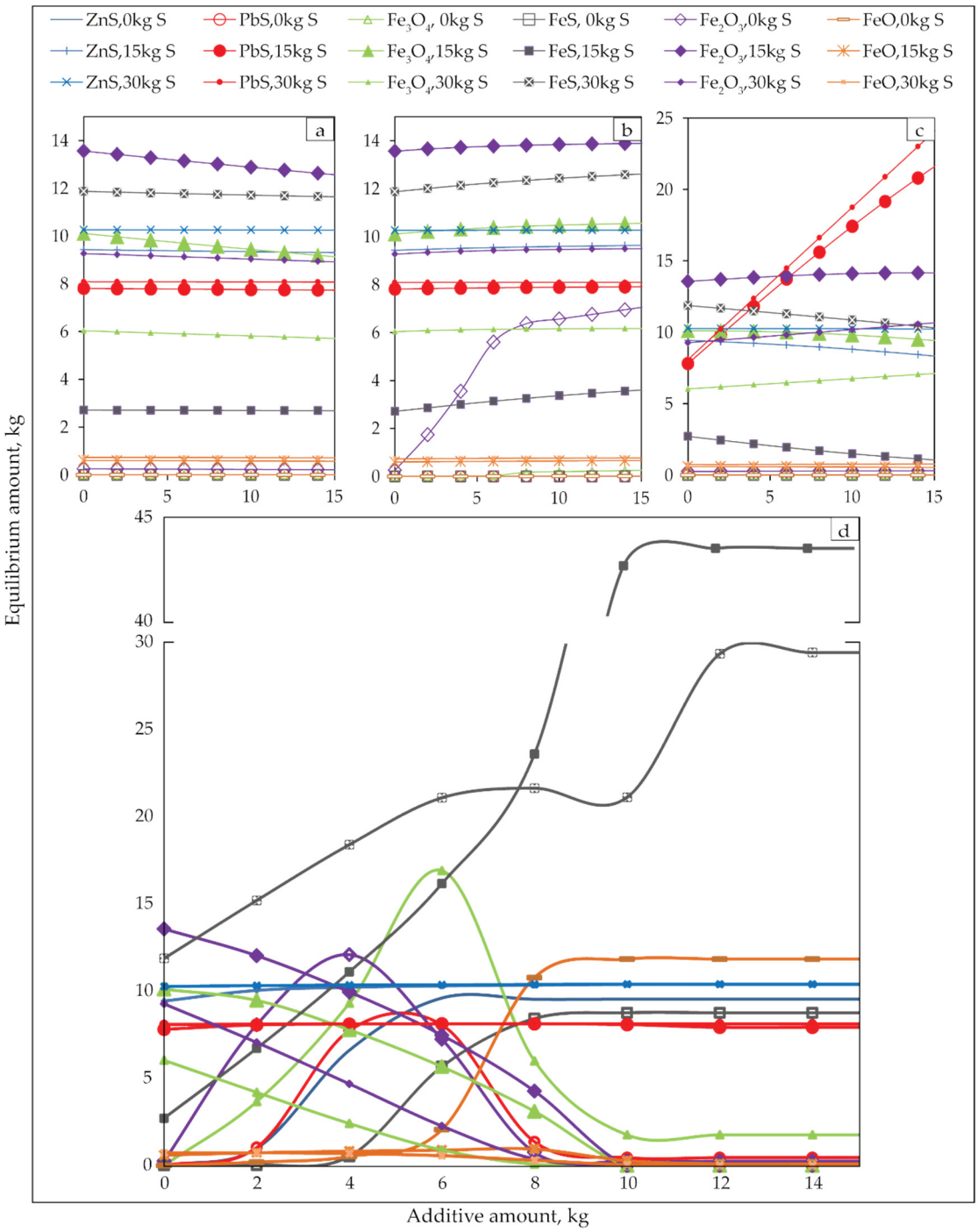

Figure 10. Equilibrium amounts of the products of sulfidization as functions of sulfidization agents and different additives (**a**) Na_2CO_3, (**b**) Cu_5FeS_4, (**c**) PbO, and (**d**) C at 550 °C.

As can be seen from Figure 10, the Na_2CO_3 additive does not influence product phase amount. Cu_5FeS_4 as additives increased Fe_2O_3 without S addition. The PbO additive has increased the PbS phase amount. Compared to other additives, the addition of carbon has the most significant effect on the amount of the product phases on temperature (550 °C).

3.2.3. Effects of Carbon Addition

According to the jarosite-PbAg sludge phases composition, with regard to the main constituents metals Equations (24)–(31), the following chemical reactions were considered in the sulfidization process (Table 5).

Table 5. Equations of jarosite-PbAg sludge with carbon and with carbon and sulfur.

Group	Equations	No.
Reactions with C	$3ZnFe_2O_4 + C = 3ZnO + 2Fe_3O_4 + CO(g)$	(24)
	$1.5Fe_2(SO_4)_3 + 5C = Fe_3O_4 + 5CO(g) + 4.5SO_2(g)$	(25)
	$3Fe_2O_3 + C = 2Fe_3O_4 + CO(g)$	(26)
	$PbSO_4 + C = PbO + CO(g) + SO_2(g)$	(27)
Reactions with C and S	$4ZnFe_2O_4 + 4C + 13S = 4ZnS + Fe_3O_4 + 4CO(g) + 5FeS + 4SO_2(g)$	(28)
	$3Fe_2(SO_4)_3 + 3C + 4.25S_2(g) = Fe_3O_4 + 3CO(g) + 14.5SO_2(g) + 3FeS$	(29)
	$Fe_2O_3 + C + 1.5S_2(g) = CO(g) + 2FeS + SO_2(g)$	(30)
	$PbSO_4 + 2C + S = PbS + 2CO(g) + SO_2(g)$	(31)

Reactions presented with Equations (24)–(31) are theoretically possible from the thermodynamic point of view and proceed spontaneously at temperatures higher than 600 °C ($\Delta_rG^\theta < 0$), as shown in Figure 11 and Table 5.

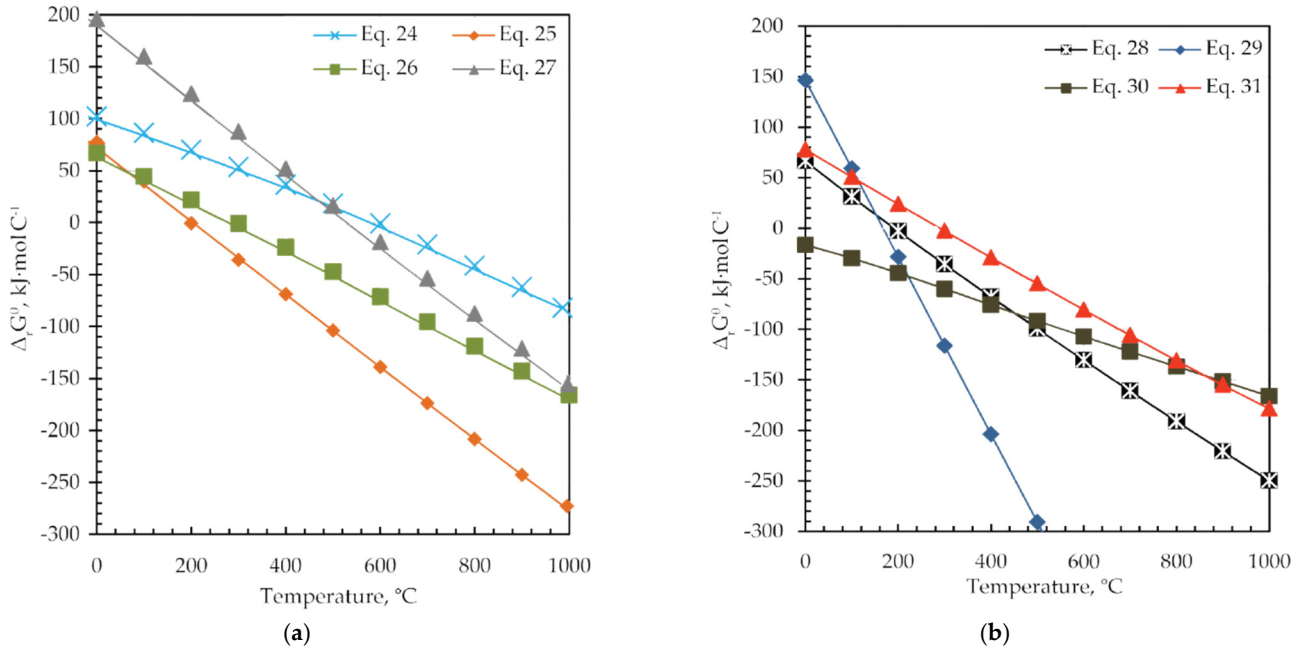

Figure 11. The change in standard Gibbs free energy (Δ_rG^θ) versus temperature for (**a**) Equations (24)–(27) and (**b**) Equations (28)–(31).

Figure 12 shows the effects of carbon and sulphur dosage on the sulfidization of jarosite-PbAg sludge at 550 °C and 900 °C.

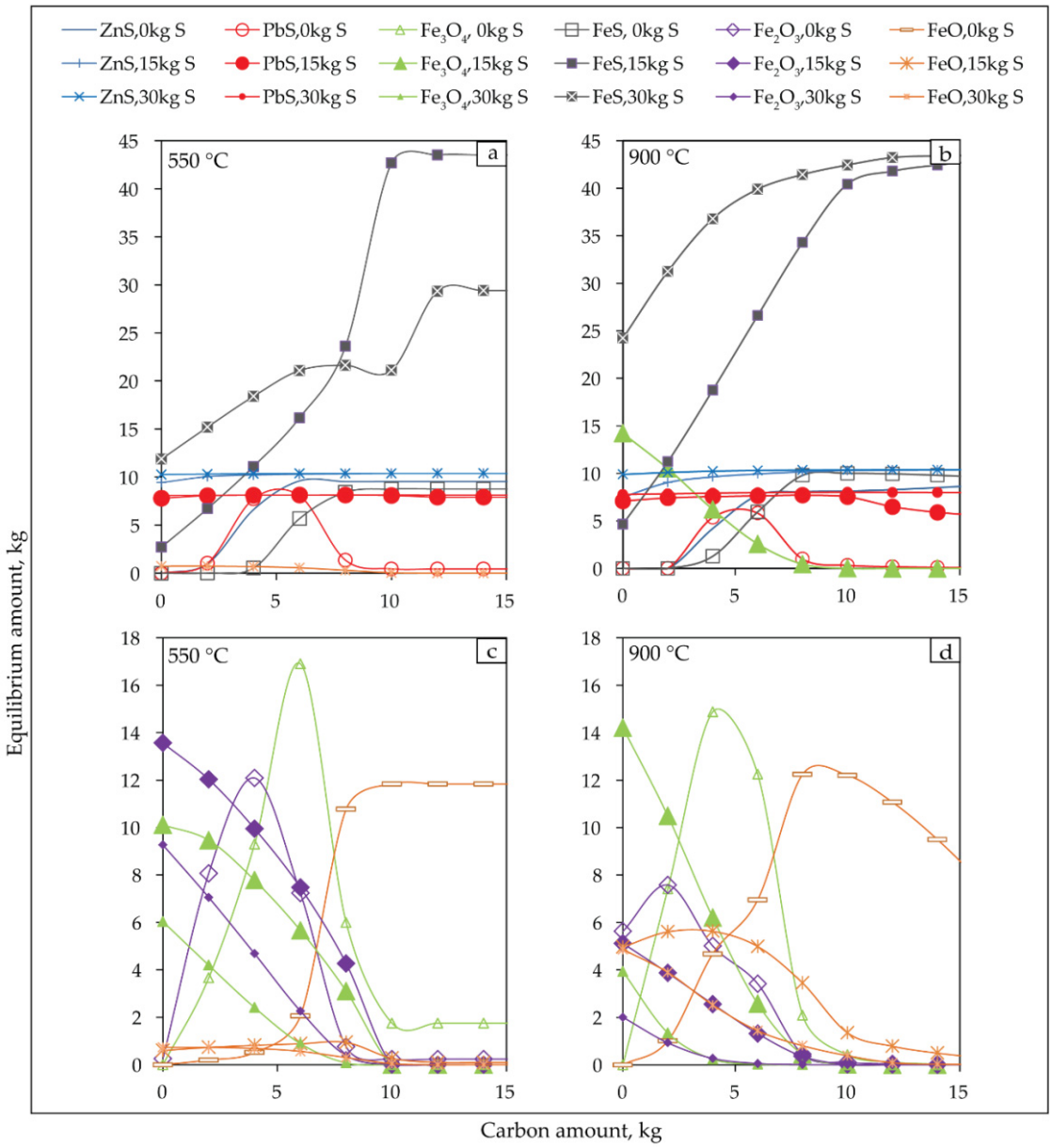

Figure 12. Equilibrium amounts of the sulphide (**a**,**b**) and oxide products (**c**,**d**) of sulfidization jarosite-PbAg sludge as functions of carbon and sulfur dosage, and temperature 550 °C (**a**,**c**) and 900 °C (**b**,**d**).

The predominance area diagram of the Zn-S-O, Pb-S-O, and Fe-S-O system at 550 °C was plotted, as shown in Figure 13. The low P_{O2} is shown to benefit Pb and Zn sulfides' stability, while oxides tend to be stable under relatively high P_{O2}. It was found that the decrease in the O_2 partial pressure was favorable for the synthesis of ZnS and PbS. Under low P_{O2}, Pb and Zn sulfides are stable in the wide range of P_{SO2}. At relatively high P_{O2}, a high P_{SO2} benefits the occurrence of Zn and Pb sulfates. On the contrary, low P_{SO2} is advantageous to stabilize the Pb and Zn oxides.

The stability region of PbS and ZnS could be achieved by lowering the O_2(g) partial pressure, which could be realized by the addition of reducing agents like carbon.

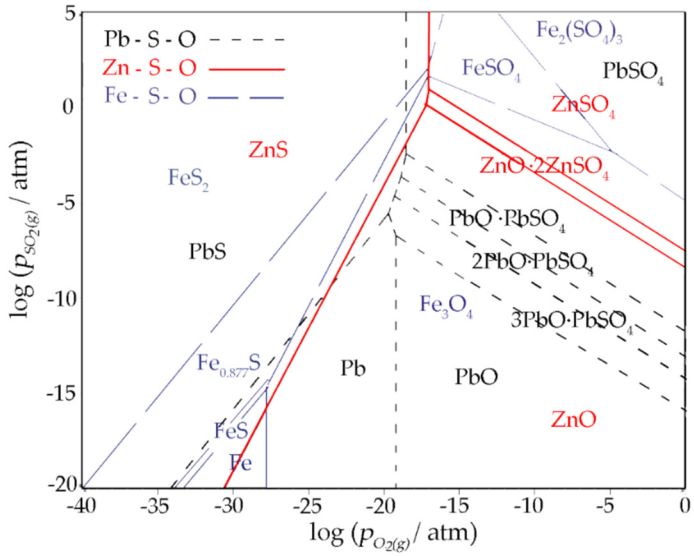

Figure 13. The predominance area diagram of Zn-S-O, Pb-S-O and Fe-S-O system at 550 °C.

The standard Gibbs free energy changes of the reactions in the range of 500 to 1000 °C were calculated for 1 mol of O_2(g) by HSC software, and the results are shown in Figure 14. It can be seen that the standard Gibbs free energy changes of the reactions Equations (34) and (35) are significantly more negative than the reactions Equations (32) and (33). That fact means that the carbon first reacts with residual oxygen, which is advantageous to inhibit the oxidation of the generated Zn and Pb sulfides during the roasting process. In addition, C is shown to favor the formation of iron oxides.

$$ZnS + 1.5O_2(g) = ZnO + SO_2(g) \quad (32)$$

$$PbS + 1.5O_2(g) = PbO + SO_2(g) \quad (33)$$

$$C + O_2(g) = CO_2(g) \quad (34)$$

$$2C + O_2(g) = 2CO(g) \quad (35)$$

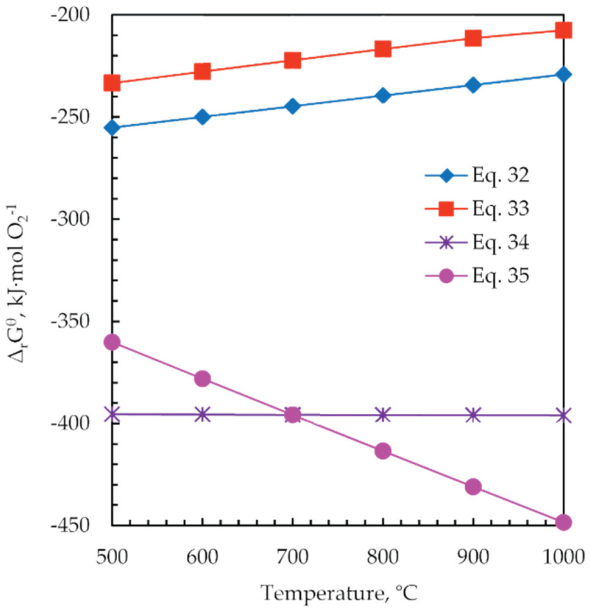

Figure 14. The change in standard Gibbs free energy (Δ_rG^θ) versus temperature for the reactions during the roasting process Equations (32)–(35).

Temperatures higher than 700 °C favor the reaction of forming CO gas, thus contributing to removing the excess of oxygen, so the temperature of roasting 900 °C was chosen.

3.3. Characterization of the Sulphidized Materials

The phase composition of the sulphidized samples was confirmed by X-ray diffraction analyses and presented in Figure 15. The results revealed that the main components of sulfidized samples are: magnetite (Fe_3O_4, JCPDS no. 96-900-5842), hematite (Fe_2O_3, JCPDS no. 96-900-0140), galena (PbS, JCPDS no. 96-500-0088), sphalerite (ZnS, JCPDS no. 96-101-1196), troilite (FeS, JCPDS no. 96-100-9044), quartz (SiO_2, JCPDS no. 96-412-4049) and lead (Pb, JCPDS no. 96-101-1120).

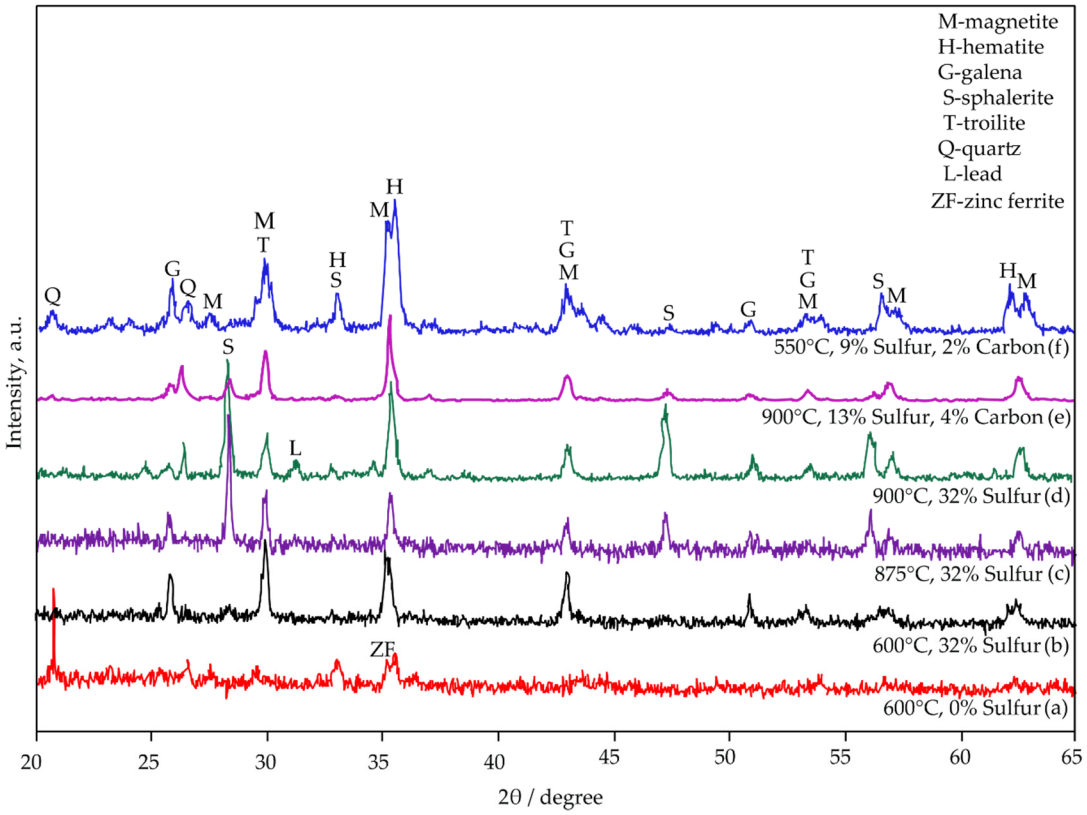

Figure 15. XRD patterns of sulfidized samples. Jarosite roasted at 600 °C (**a**), jarosite with 32.00% of added sulfur roasted at 600 °C (**b**), 875 °C (**c**), 900 °C (**d**), jarosite with 13.00% of sulfur and 4.00% of added carbon roasted at 900 °C (**e**), and jarosite with 9.00% of sulfur and 2.00% of added carbon roasted at 550 °C (**f**).

It is evident that sulfur addition has an insignificant effect on the sulfidization of Zn at lower temperatures (600 °C) (Figure 15a,b), even if sulfur is added in excess. The sphalerite content increases with the increase in temperature (Figure 15c,d), indicating that high-temperature roasting is beneficial for the sulfidization of zinc. It could be concluded that high temperatures and sulfur's addition promote Zn sulphidation (Figure 15d), and, at temperatures higher than 600 °C, formations of intensive peaks at 2θ 28°, 47°, and 56° could be attributed to sphalerite (Figure 15b–d). For lead, sulphidation temperatures (600–875 °C) are optimal because, at higher temperatures (900–950 °C), elemental lead is present as a product (Figure 15d).

At lower temperatures and 2.00 wt.% addition of carbon (Figure 15f), higher intensities of magnetite and hematite peaks are observed concerning higher temperatures and carbon additions (Figure 15e), indicating that this process is favorable for further treatment of sulfidized material by magnetic separation. The results obtained by XRD analysis are in accordance with the thermodynamic calculations.

Chemical composition and weight loss for sulfidized samples are presented in Table 6 for various charge compositions and process parameters.

Table 6. Chemical composition (wt.%) and weight loss (Δm) of sulfidized jarosite-PbAg sludge.

No	Sample	Fe	Pb	Zn	S	Al_2O_3	SiO_2	CaO	Cu	Ag
Addition of Sulfur										
regime: 135 °C, 260 °C, 360 °C, 460 °C, 600 °C/30 min, 900 °C/3 h										
1	68/32_S	43.65	6.45	8.03	7.17	2.93	16.73	3.20	0.80	0.05
2	73/27_S	41.32	6.13	7.96	6.81	2.93	16.73	3.20	0.80	0.04
3	78/22_S	40.15	5.98	7.80	6.63	2.92	16.72	3.20	0.78	0.03
4	83/17_S	43.03	5.80	6.81	6.76	2.93	16.73	3.20	0.50	0.02
5	88/12_S	43.76	5.10	5.36	6.44	2.89	16.54	3.16	0.47	0.02
6	93/7_S	43.98	4.92	4.93	6.35	2.94	16.81	3.22	0.64	0.03
7	98/2_S	43.57	4.22	4.86	5.97	2.83	16.19	3.10	0.36	0.01
Addition of Sulfur and Carbon										
regime: 135 °C, 260 °C, 360 °C, 460 °C, 550 °C, 60 min										
8	89/9_S/2_C	39.01	5.81	5.94	8.98	2.66	15.20	2.91	0.76	0.05
9	88/8_S/4_C	43.20	4.95	6.71	10.26	3.19	18.23	3.49	0.92	0.05
10	83/13_S/4_C	40.71	6.45	7.28	10.46	3.03	17.32	3.31	0.85	0.04
11	78/18_S/4_C	39.82	4.53	6.42	9.57	2.94	16.81	3.22	0.85	0.05
12	83/7_S/10_C	41.29	5.23	6.78	10.11	3.05	17.42	3.33	0.58	0.02
13	61/29_S/10_C	36.80	8.70	6.40	9.77	2.71	15.53	2.97	0.54	0.03
regime: 135 °C, 260 °C, 360 °C, 460 °C, 600 °C/30 min, 900 °C/3 h										
14	66/24_S/10_C	37.68	8.22	7.01	10.12	2.78	15.90	3.04	0.62	0.02
15	71/19_S/10_C	40.09	7.71	7.37	10.56	2.96	16.92	3.24	0.64	0.02
16	76/14_S/10_C	38.34	7.36	7.88	10.02	2.83	16.18	3.10	0.58	0.02
17	81/9_S/10_C	41.54	7.02	8.54	11.20	3.04	17.41	3.33	0.75	0.05
18	86/4_S/10_C	42.12	1.21	4.90	8.64	3.11	17.78	3.40	0.81	0.03
19	88/2_S/10_C	43.38	0.67	2.96	7.78	3.20	18.31	3.50	0.62	0.02
Addition of Sulfur and Additives										
regime: 135 °C, 260 °C, 360 °C, 460 °C, 550 °C, 30 min										
20	83/17_S/10_Na_2CO_3	36.59	5.80	6.27	9.22	2.70	15.44	2.95	0.84	0.05
21	83/17_S/10_bornite	35.21	4.84	6.32	8.90	2.60	14.86	2.84	1.91	0.06
22	83/17_S/10_PbO	29.56	6.17	5.94	8.11	2.18	12.48	2.39	0.80	0.04
Sulfidization of $ZnFe_2O_4$ with Addition of Sulfur and Carbon										
regime: 135 °C, 260 °C 360 °C, 460 °C, 500 °C, 30 min										
23	83_$ZnFe_2O_4$/17_S	46.05		16.93	10.95					
regime: 135 °C, 260 °C, 360 °C, 460 °C, 600 °C/30 min, 900 °C/1 h										
24	78_$ZnFe_2O_4$/22_S	49.24		2.34	3.97					
25	71_$ZnFe_2O_4$/19_S/10_C	43.89		12.10	8.45					
26	83/17_S -pressed	51.48	5.49	11.23	10.79	2.23	12.78	2.44	1.11	0.05

Samples are labeled as following:

J/S/C/A

where J means the amount of jarosite or $ZnFe_2O_4$ (%), S means the amount of sulfur (%), C means the amount of carbon (%), and A means the amount of additive (%).

According to the results presented in Table 6, it could be concluded that an increase of sulfur addition promotes sulfidization of jarostite-PbAg sludge (Samples 1–7). The addition of carbon in the sulfidization mixture promotes sulfidization at lower sulfur additions and at lower process temperatures. The best results for the addition of 4.00% of carbon are for sample 10 with 13.00% of sulfur and 4.00% of added carbon. With higher addition

of carbon and lower sulfur at higher temperatures, the content of zinc and lead increase up to 9.00% of sulfur at 10.00% of carbon, and with a further decrease of sulfur results shows a rapid decrease of sulfide quality. For samples with 2.00–4.00% of sulfur, this is the most prominent. A possible reason for quality decrease could be the formation of non-stoichiometric lead silicates below the detection limit for XRD.

Additives do not have a significant effect on sulfide quality, so, for further investigations only samples with sulfur and carbon were used.

Results of sulfidization of synthesized $ZnFe_2O_4$ showed that lower sulfur addition promotes the formation of zinc sulfides; however, the addition of carbon has an adverse impact on sulfidization results. These experiments were performed to verify the possibility of sulfidization of pure materials but were not considered further as the Jarostite-PbAg sludge is a complex system, and the behavior of individual compounds does not represent a realistic situation. Pressing of jarosite-PbAg sludge before sulfidization gives promising results for further investigations.

Size distribution data of sample 81/9_S/10_C, which will be used for flotation, obtained from laser diffraction measurements are plotted as a particle and cumulative size distribution shown in Figure 16. It is shown that the median diameter of particles is 9.37 µm.

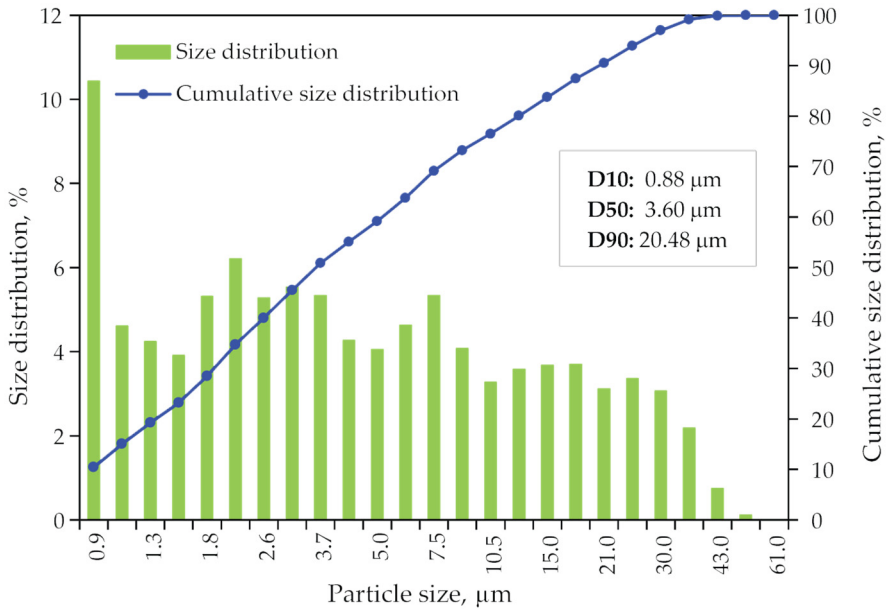

Figure 16. Particle size distribution and the cumulative size distribution for the sample prepared for the flotation process.

Optical microscopy of sulfidized jarosite-PbAg sludge, with the addition of sulfur (sample no 1-68/32_S) presented in Figure 17, shows that sphalerite and galena exist in the form of intergrowths (simple and complex). The size of intergrown aggregates is bigger than 100 µm, but individual mineral grains ranging from 10 to 20 µm. The most common copper phases are elemental Cu, chalcocite, and covellite, while chalcopyrite is the least represented. Similar to the previous case, these phases almost always occur in the form of intergrowths and inclusions, and that elemental copper ranges some 30 µm. The chalcocite/covellite individual grains with over 50 µm in length were also determined.

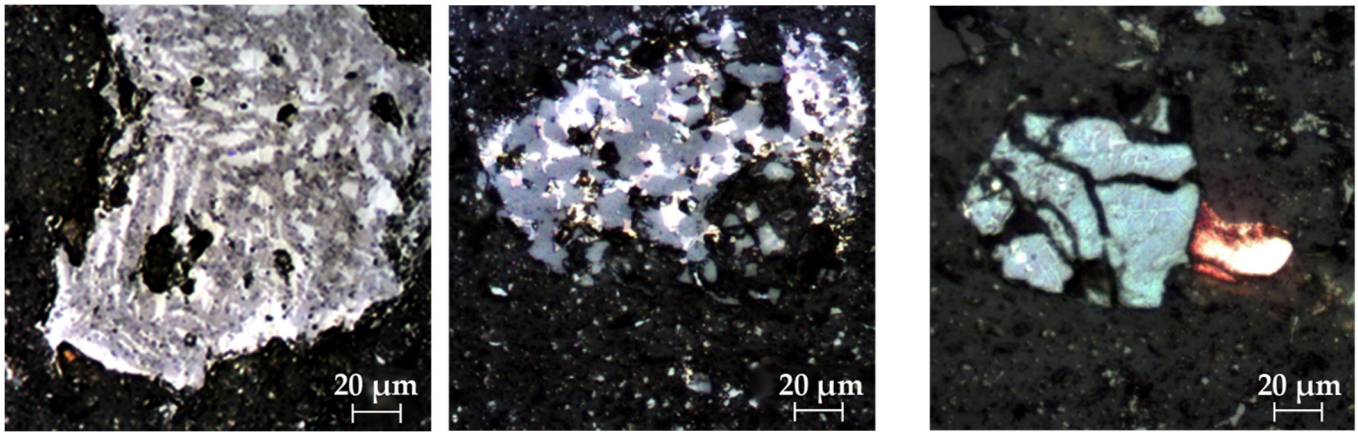

The simple intergrowth of galena and sphalerite

The complex intergrowth of galena, sphalerite, pyrrhotite and pyrite

The intergrowth of chalcocite/covellite and elemental Cu

Figure 17. Optical microscopy of sulfidized jarosite-PbAg sludge with the addition of sulfur.

According to the optical microscopy study of sulfidized jarosite-PbAg sludge, with the addition of sulfur and carbon (sample no 10-83/13_S/4_C) mineral grains of galena, sphalerite, elemental iron and copper, spinel phases, hematite, and magnetite were determined (Figure 18). Galena was mostly in liberated form, ranging from 10 to more than 70 μm. It is characteristic that it contains tendril of sphalerite and elemental Fe. Elemental Fe occurs in samples in the form of liberated grains bigger than 20 μm, but also in the form of microinclusions in galena. Sphalerite is less abundant, appearing in a form of liberated grains, inclusions, and simple intergrowths with galena. The size of liberated grains of sphalerites is up to 40 μm.

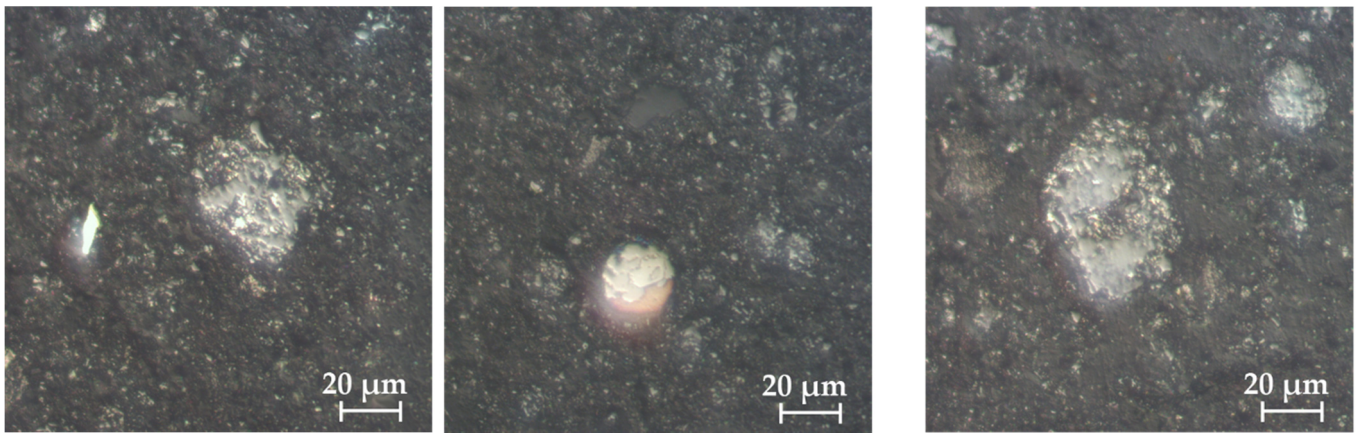

The liberated grain of galena with elemental Fe

The simple intergrowths of elemental Fe and Cu

The liberated grain of galena with segregation of sphalerite

Figure 18. Optical microscopy of sulfidized jarosite-PbAg sludge with the addition of sulfur and carbon.

The optical microscopy study of sulfidized jarosite-PbAg sludge, with the addition of sulfur and carbon for magnetic separation (sample no 8-89/9_S/2_C) is given in Figure 19, showing mineral grains of galena, sphalerite, elemental iron and copper, spinel phases, hematite, magnetite, and graphite. The most common mineral is galena, occurring mostly in liberated grains, in the range from 10 to more than 250 μm. Sphalerite is rare, appearing in the form of liberated grains, inclusions, and simple intergrowths with galena. Elemental copper is also rare occurring in the form of simple intergrowths with elemental iron.

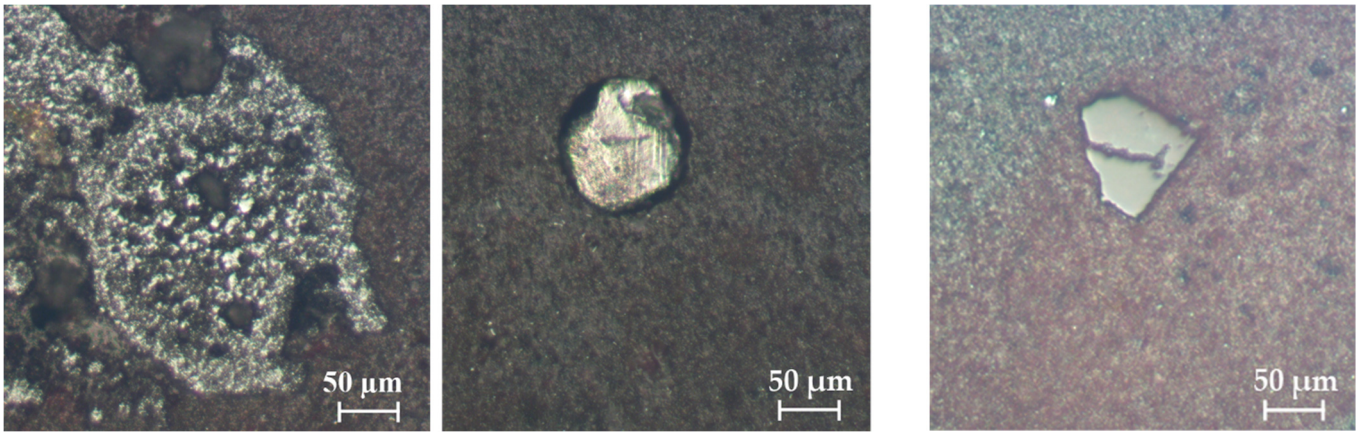

The galena in the sample | The galena in the sample | The spinel phase in hematite

Figure 19. Optical microscopy of sulfidized jarosite-PbAg sludge with the addition of sulfur and carbon for magnetic separation.

3.4. Magnetic Separation

Results of magnetic separation performed on samples 89/9_S/2_C did not yield any positive and promising results, i.e., samples consist of 96–100% of the magnetic fraction when grounded samples to −37µm and magnetic field strength 700 G are used.

Heterogeneous mineral phases were obtained (Figure 19) due to sulfidization of jarosite, so the results of separation of sulfide minerals by magnetic separation are below the values that allow practical application.

Based on the mineral composition, as well as the structural and textural characteristics of sulfidized samples, it was determined that sulfide minerals do not appear in the elemental form with idiomorphic grains suitable for concentration. Very small, but significantly present iron minerals, usually magnetite, are impregnated in them.

The determined texture of sulfidized jarosite-PbAg sludge does not allow the liberation of minerals, even by applying maximum size reduction levels. This is the main reason and a serious obstacle for the concentration of Zn and Pb sulfides by magnetic separation.

3.5. Flotation

Flotation tests were performed at samples with and without addition of different amounts of carbon (4 and 10%). The following samples were used: 68/32_S, 83/13_S/4_C, and 81/9_S/10_CA. Samples 68/32_S and 83/13_S/4_C; and 81/9_S/10_C were grounded using ball mill to -63; and -37 µm, respectively, before flotation tests. Results of flotation tests are presented in Table 7 and represent the mean values of the three tests.

Table 7. Results of flotation tests (U-input material, K-concentrate, J-tailings).

Sample	Weight, %	Composition, wt.%					Distribution, %				
		Pb	Zn	Fe	Cu	Ag	Pb	Zn	Fe	Cu	Ag
0% C (68/32_S; +63 μm)											
U	100.00	6.45	8.03	43.65	0.80	0.050	100.00	100.00	100.00	100.00	100.00
K	75.44	7.13	6.52	43.15	0.76	0.050	83.40	61.26	74.57	71.91	75.58
J	24.56	4.37	12.67	45.32	0.91	0.050	16.65	38.74	25.50	28.01	24.42
0% C (68/32_S; −63+37 μm)											
U	100.00	6.31	7.96	41.82	0.78	0.045	100.00	100.00	100.00	100.00	100.00
K	70.18	8.08	8.77	40.86	0.85	0.043	89.92	77.35	68.57	76.83	66.73
J	29.82	2.13	6.06	44.09	0.61	0.050	10.08	22.69	31.44	23.15	33.27
0% C (68/32_S; −37 μm)											
U	100.00	6.30	7.85	41.80	0.77	0.05	100.00	100.00	100.00	100.00	100.00
K	54.28	11.19	11.83	39.47	1.12	0.05	91.24	81.79	51.26	79.30	54.28
J	45.72	5.73	3.13	44.56	0.35	0.05	8.76	18.21	48.74	20.70	45.72
4% C (83/13_S/4_C; −63 μm)											
U	100.00	6.45	7.28	41.03	0.85	0.04	100.00	100.00	100.00	100.00	100.00
K	8.75	4.72	4.05	19.87	1.58	0.04	6.40	4.87	4.24	16.26	10.25
J	91.25	6.62	7.59	43.06	0.78	0.04	93.60	95.14	95.76	83.74	89.75
10% C (81/9_S/10_C; −37 μm)											
U	100.00	7.02	8.54	41.26	0.78	0.05	100.00	100.00	100.00	100.00	100.00
KPb	15.89	11.49	6.05	31.62	0.79	0.04	26.00	11.26	12.17	16.09	14.47
KZn	25.48	6.47	9.27	44.86	0.63	0.05	23.46	27.65	27.70	20.58	26.32
J	58.64	6.05	8.89	42.31	0.84	0.05	50.54	61.09	60.13	63.34	59.20

Presented results show that, with the increase of particle size for sample 68/32_S, flotation efficiency increases for all investigated elements, except for silver. However the mass efficiency for this sample is not favorable.

From all the presented flotation tests, it could be concluded that flotation is not a feasible route for the treatment of sulfidized jarosite-PbAg sludge. All elements of interest are mainly concentrated in tailings instead of in the concentrate. These results do not prove the data available in the literature and are presented in Table 1.

Textural and complex morphological and multi-mineral phase changes, similar to the samples for the magnetic separation, were noticed, preventing efficient flotation of sulfide minerals (Figures 17 and 18). Similar to the previous case, sphalerite and galena do not appear in their pure form. Small iron minerals were embedded in them and around the grain rims—in the first place, magnetite. The appearance of metallic (elemental) iron droplets is also interesting (Figure 18).

3.6. Smelting

Results of submerged DC plasma processing of dried jarosite-PbAg sludge and composition of final products matte, filter cake, and slag are presented in Table 8. From process mass balance and composition of final products, distribution coefficients were derived and also presented in Table 8.

Table 8. Compositions and distribution coefficients of final products of the submerged plasma process.

Elem/Comp.	Composition, wt.%			Distribution, %		
	Matte	**Filter Cake**	**Slag**	**Matte**	**Filter Cake**	**Slag**
Zn	2.24	17.95	2.52	5.21	79.43	15.36
Pb	0.48	18.92	1.16	1.22	91.10	7.68
Cu	3.01	0.81	0.64	48.18	24.83	26.99
Fe	38.87	7.06	30.70	29.27	10.12	60.61
S	21.00	8.18	4.63	43.11	31.96	24.92
CaO	1.11	1.85	13.43	2.77	8.82	88.40
MgO	0.10	0.17	1.54	2.23	7.08	90.69
SiO_2	1.71	2.18	22.20	2.67	6.48	90.85
Al_2O_3	0.26	0.38	4.70	1.99	5.40	92.61
MnO	0.59	0.20	1.22	14.20	9.01	76.80
Na_2O	0.12	1.94	0.42	2.47	75.22	22.31
K_2O	0.16	0.23	0.39	9.77	27.18	63.05
C	0.14	10.60	0.35	0.66	95.02	4.32
Ag	0.09	0.09	0.03	26.92	52.86	20.22
Ge	0.00	0.05	0.01	0.41	86.17	13.41
In	0.01	0.04	0.00	8.90	81.82	9.29

The zinc content in the final slag is relatively low. Some of the remaining Zn in the slag can be, however, in the form of matte droplets that are accounted as a physical matte loss. This can be concluded by looking at the S content of the slag, which is expected that Zn will always, to some extent, be distributed into the matte phase. The matte phase contains 2.24% zinc, as shown in the analyzed results. Almost all of the Pb was removed from the slag by fuming; only Pb traces were distributed into the matte phase. The distribution of the compounds during the test is more or less as expected.

Based on the presented results of slag chemistry, it could be concluded that the addition of lime or limestone is not necessary to adjust the slag chemistry. The calculated slag basicity was 0.55. Without the added flux, it is estimated that the slag temperature would be 1150–1200 °C. By removing the lime, a higher temperature of slag will be obtained, which should only provide better fuming conditions; excellent fuming results are obtained at low slag temperatures.

Using 10.00% of coke in the charge, poor Cu matte (low in Cu content) was obtained. This is because too much SO_4 was reduced to elemental S, which then distributes and creates an excess of matte, first combining with copper and later iron. This can be corrected by lowering the carbon addition in the feed by adding some copper-containing materials or reducing the carbon addition. In addition, the distribution of Ag is not favorable in this process.

Prior to the smelting of sulfidized jarosite-PbAg sludge in a submerged DC arc furnace, laboratory-scale experiments were performed in a chamber furnace. The first set of experiments were performed with jarosite sulfidized only with the addition of sulfur, while the second set was performed on samples of jarosite sulfidized with the addition of sulfur and carbon.

As optimal samples for the smelting test, samples 86/14_S and 83/13_S/4_C were used.

Smelting experiments in each set were repeated three times, and Tables 9 and 10 present mean values. From process mass balance and composition of final products, distribution coefficients were derived and presented in respective tables.

Table 9. Results of smelting tests, jarosite-PbAg sludge sulfidized with the addition of sulfur.

Elem/Comp.	Composition, wt.%			Distribution, %		
	Slag	Matte	Dust	Slag	Matte	Dust
Zn	1.20	5.83	78.71	7.36	23.42	69.22
Pb	0.03	12.76	12.07	0.26	82.63	17.11
Fe	63.79	39.20		71.36	28.64	
Cu	0.00	2.06	0.01	0.20	99.68	0.12
S	0.00	38.05	3.47	0.01	69.26	1.38
Al_2O_3	5.06	0.17	0.08	97.63	2.15	0.22
SiO_2	29.29	0.77	0.02	98.30	1.69	0.01
Ag	0.00	0.37		0.02	99.98	

Table 10. Results of smelting tests, with jarosite-PbAg sludge sulfidized with the addition of sulfur and carbon.

Elem/Comp.	Composition, wt.%				Distribution, %			
	Slag	Matte	Pb	Dust	Slag	Matte	Pb	Dust
Zn	1.13	2.75	8.20	81.64	9.26	4.02	15.00	71.72
Pb	0.21	2.24	36.06	2.22	2.31	4.50	90.52	2.67
Fe	56.72	44.19	0.16		87.74	12.21	0.05	
Cu	0.04	6.38	0.00	0.01	3.12	96.73	0.05	0.10
S	1.73	41.50	51.44	8.21	5.28	22.59	35.00	2.68
Al_2O_3	4.52	0.03		0.13	99.57	0.13		0.30
SiO_2	25.99	0.45		0.02	99.68	0.31		0.01
Ag	0.00	0.17	0.85		0.01	13.59	86.40	

As it could be seen in Table 9 and Figure 20, separation of slag and matte is not adequate. Zinc and lead are distributed between three phases, indicating the inefficiency of this process with respect to future valorization. The only concentrations which could be considered as favorable are copper and silver; they concentrate in the matte phase.

Figure 20. Products of 86/14_S smelting.

From the presented results, it could be concluded that zinc is concentrated in the matte phase, while one-fourth of silver is vaporized and collected in the dust phase. Lead is distributed between the matte and lead phase, and iron is distributed between slag and matte. Copper is mainly concentrated in the matte phase. The difference of S up to 100% in distribution is due to the formation of SO_2(g). The presence of carbon in the smelted sample promotes the formation of the lead phase. Formation of the lead phase is significant, since Pb metal is a known metal-collector for silver, and as presented in Table 10, over 50% is collected in this phase.

From Figure 21, it could be seen that the slag and matte phases are properly separated. The lead phase was also easily separated from the bottom of the matte. Dust phase mainly composed of zinc oxide is collected at the top of the crucible.

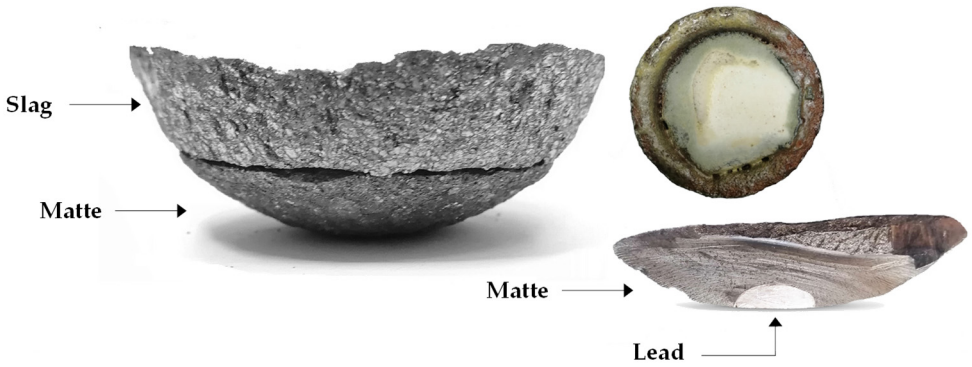

Figure 21. Final products of 83/13_S/4_C smelting.

Based on the laboratory smelting results, semi-industrial smelting was performed on sulfidized jarosite-PbAg sludge with the addition of 13.00% of sulfur and 4.00% of carbon. Results are presented in Table 11.

Table 11. Submerged DC arc furnace smelting of 83/13_S/4_C.

Elem/Comp.	Composition, wt.%				Distribution, %			
	Slag	Matte	Pb	Dust	Slag	Matte	Pb	Dust
Zn	1.07	3.60	0.29	77.06	8.36	3.13	0.27	88.24
Pb	0.27	4.03	98.92	3.36	2.05	3.46	90.52	3.80
Fe	49.03	50.83	0.23		89.62	10.32	0.05	
Cu	0.03	8.32	0.00	0.02	2.90	96.77	0.03	0.30
S	0.61	31.58	0.39	2.17	4.36	24.93	0.03	2.31
Ag		0.04	0.28		0.01	10.73	89.23	
In	0.00	0.02	0.01		1.98	66.20	31.82	
Ga	0.00	0.07	0.01		1.82	85.96	12.22	
Al_2O_3	3.68	0.05		0.01	99.82	0.16		0.02
SiO_2	25.71	0.65		0.02	99.71	0.28		0.01
CaO	5.51	0.52		0.01	98.95	1.03		0.02
MgO	0.46		0.01		99.56	0.32	0.12	
MnO	2.00	0.27	0.15	0.04	89.35	10.20	0.36	0.09

Presented results in Table 11 are comparable to the results presented in Table 10 for laboratory smelting. The majority of Fe is concentrated in the slag phase with calculated basicity of 0.20. The lead phase was formed, and it is comprised of Pb with collected Ag and some quantity of iron. The matt phase presents a mixture of Fe-Zn-Pb-Cu sulfides. It could be further treated by the ISP process, if locally available, or additional synergetic materials should be added in the charge to further promote distribution, so the majority of valuable components is concentrated in one phase. Input material represents Zn-Pb non-standard residue with a high sulfur content and presence of contaminants (Cd and As) requiring a specific off-gas treatment designed according to BAT techniques, i.e., quenching, baghouse filter, scrubbing, and optionally absorption.

4. Conclusions

According to the presented results, it could be concluded that jarosite Pb/Ag sludge is a very complex raw material and very challenging to processing—for example, material drying and pretreatment of feed mix to reduce energy consumption.

It is shown that it is not possible to perform magnetic separation and flotation of sulfidized material in spite of some results presented in the available scientific literature.

The obtained texture of sulfidized jarosite does not allow the liberation of minerals, which influences further processing efficiency.

Smelting with lead phase is a viable option, with the addition of synergetic raw materials. The formation of the lead phase is favorable for the concentration of precious metals and REE.

Added value for the suggested sulfidization route could be the utilization of ammonia, sulfur from off-gas fixation, and production of sulfate salt. Additional work in this technological phase for determination of kinetics and mechanism of the process will be a logical continuation of research efforts.

The presented experimental work confirmed that secondary Pb/Zn materials are easily handled in electric furnaces; energy for smelting is transferred to the slag from the submerged electrodes.Because of lead melting points and aggressive slags, the design of furnace lining is crucial. Due to its composition, smelting of jarosite-PbAg sludge could be fluxless for obtaining appropriate oxide system, energy input, and slag conductivity and to enable good separation between smelted products.

The proposed process offers the technological capability to separate nonvaluable elements from valuables and collect the latter in higher concentration products, more suitable for downstream refiners, which could also be interesting in the case of complex, polymetallic, and refractory primary materials processing.

Future efforts in extractive metallurgy will be related to the development of new technologies, more likely fragments or niches, allowing the production of minor and critical metals, such as REE, PGMs, and technological metals from non-standard raw materials, which is crucial for achieving industrial sector sustainability.

Author Contributions: Ž.K. and M.K. conceptualized and managed the research and co-wrote the paper together with other co-authors. N.G. performed the thermodynamic calculations. S.J. participated in the analysis and discussion of the obtained results and co-wrote this paper. M.S. and J.S. helped in the discussion of the results and co-wrote this paper. All authors have read and agreed to the published version of the manuscript.

Funding: This work was financially supported by the Ministry of Education, Science and Technological Development of the Republic of Serbia (Contract No. 451-03-68/2020-14/200135).

Conflicts of Interest: The authors declare no conflict of interest.

References

1. International Lead and Zinc Study Group. Available online: http://www.ilzsg.org/static/statistics.aspx (accessed on 22 June 2020).
2. Monhemius, J. The Iron Elephant: A Brief History of Hydrometallurgists' Struggles with Element No.26. In Proceedings of the XXVIII International Mineral Processing Congress (IMPC 2016), Quebec City, QC, Canada, 11–15 September 2016.
3. Cusano, G.; Gonzalo, M.R.; Farrell, F.; Remus, R.; Roudier, S.; Sancho, L.D. *Best Available Techniques (BAT) Reference Document for the Main Non-Ferrous Metals Industries*; Industrial Emissions Directive 2010/75/EU (Integrated Pollution Prevention and Control); European Commission: Seville, Spain, 2017.
4. Komnitsas, C.; Pooley, F.D. Bacterial oxidation of an arsenical gold sulphide concentrate from Olympias, Greece. *Miner. Eng.* **1990**, *3*, 295–306. [CrossRef]
5. Tabelin, C.B.; Corpuz, R.D.; Igarashi, T.; Villacorte-Tabelin, M.; Alorro, R.D.; Yoo, K.; Hiroyoshi, N. Acid mine drainage formation and arsenic mobility under strongly acidic conditions: Importance of soluble phases, iron oxyhydroxides/oxides and nature of oxidation layer on pyrite. *J. Hazard. Mater.* **2020**, *399*, 122844. [CrossRef] [PubMed]
6. Environmental Protection Agency (EPA). *European Waste Catalogue and Hazardous Waste List*; Environmental Protection Agency (EPA): Washington DC, USA, 2002.
7. Wang, R.; Yan, Q.; Su, P.; Shu, J.; Chena, M.; Xiao, Z.; Han, Y.; Cheng, Z. Metal mobility and toxicity of zinc hydrometallurgical residues. *Process Saf. Environ. Prot.* **2020**, *144*, 366–371. [CrossRef]
8. Kangas, P.; Nyström, M.; Orko, I.; Koukkari, P.; Saikkonen, P.; Rastas, J. *The Jarogain Process for Metals Recovery from Jarosite and Electric Arc Furnace Dust—Process Design and Economics*; VTT Technical Research Centre of Finland Ltd.: Espoo, Finland, 2017; p. 317.
9. Creedy, S.; Glinin, A.; Matusewics, R.; Hughes, S.; Reuter, M. Outotec Ausmelt Technology for Treating Zinc Residues. In Proceedings of the 7th European Metal Conference (EMC 2013), Weimar, Germany, 23–26 June 2013; pp. 485–493.

10. Hughes, S.; Reuter, M.A.; Baxter, R.; Kaye, A.; Hughes, S.; Reuter, M.A.; Baxter, R.; Kaye, A. Ausmelt Technology for Lead and Zinc Processing. In Proceedings of the Lead and Zinc 2008, South African Institute of Mining and Metallurgy (SAIMM), Cape Town, South Africa, 25–29 February 2008; pp. 147–162.
11. Salminen, J.; Nyberg, J.; Imris, M.; Heegaard, B.M. Smelting Jarosite and Sulphur Residue in a Plasma Furnace. In Proceedings of the 9th International Symposium on Lead and Zinc Processing (PbZn 2020), San Diego, CA, USA, 23–27 February 2020; pp. 391–403.
12. Rath, G.; Vlajcic, T.; Metelmann, O. Lead smelting in a submerged arc furnace. *JOM* **1990**, *42*, 39–40. [CrossRef]
13. Radovanović, D.; Kamberović, Ž.; Andjić, Z.; Ranitović, M.; Marković, B. The effect of CaO and MgO addition and cooling rate on stability of slag obtained after jarosite and neutral leaching residue treatment in the Waelz process. *Physicochem. Probl. Miner. Process.* **2018**, *54*, 484–495.
14. Mombelli, D.; Mapelli, C.; Di Cecca, C.; Barella, S.; Gruttadauria, A.; Ragona, M.; Pisu, M.; Viola, A. Characterization of cast iron and slag produced by jarosite sludges reduction via Arc Transferred Plasma (ATP) reactor. *J. Environ. Chem. Eng.* **2018**, *6*, 773–783. [CrossRef]
15. Wang, H.B.; Zheng, C.Z.; Qin, S.C. Study of a Novel Chloride Volatilization Process for the Treatment of Jarosite Residue. In Proceedings of the 9th International Symposium on Lead and Zinc Processing (PbZn 2020), San Diego, CA, USA, 23–27 February 2020; pp. 835–845.
16. Manojlović, V.; Kamberović, Ž.; Gajić, N. An alternative route for valorization of valuable metals from jarosite residue. *TehnikaRGM* **2019**, *74*, 388–393. [CrossRef]
17. Chai, L.; Liang, Y.; Ke, Y.; Min, X.; Tang, C.; Zhang, H.; Xie, X.; Yuan, C. Mechano-chemical sulfidization of zinc oxide by grinding with sulfur and reductive additives. *Trans. Nonferr. Met. Soc. China* **2013**, *23*, 1129–1138. [CrossRef]
18. Li, C.; Wei, C.; Deng, Z.; Li, X.; Li, M.; Xu, H. Hydrothermal Sulfidization and Flotation of Oxidized Zinc-Lead Ore. *Metall. Mater. Trans. B* **2014**, *45*, 833–838. [CrossRef]
19. Liang, Y.; Chai, L.; Min, X.; Tang, C.; Zhang, H.; Ke, Y.; Xie, X. Hydrothermal sulfidization and floatation treatment of heavy-metal-containing sludge for recovery and stabilization. *J. Hazard. Mater.* **2012**, *217–218*, 307–314. [CrossRef]
20. Li, Y.; Wang, J.; Wei, C.; Liu, C.; Jiang, J.; Wang, F. Sulfidization roasting of low grade lead–zinc oxide ore with elemental sulfur. *Miner. Eng.* **2010**, *23*, 563–566. [CrossRef]
21. Zheng, Y.; Liu, W.; Qin, W.; Jiao, F.; Han, J.; Yang, K.; Luo, H. Sulfidization roasting of lead and zinc carbonate with sulphur by temperature gradient method. *J. Cent. South Univ.* **2015**, *22*, 1635–1642. [CrossRef]
22. Han, J.; Liu, W.; Wang, D.; Jiao, F.; Qin, W. Selective Sulfidization of Lead Smelter Slag with Sulfur. *Metall. Mater. Trans. B* **2015**, *47*, 344–354. [CrossRef]
23. Han, J.; Liu, W.; Qin, W.; Zhang, T.; Chang, Z.; Xue, K. Effects of sodium salts on the sulfidization of lead smelting slag. *Miner. Eng.* **2017**, *108*, 1–11. [CrossRef]
24. Han, J.; Liu, W.; Wang, D.; Jiao, F.; Zhang, T.; Qin, W. Selective Sulfidization of Lead Smelter Slag with Pyrite and Flotation Behavior of Synthetic ZnS. *Metall. Mater. Trans. B* **2016**, *47*, 2400–2410. [CrossRef]
25. Zheng, Y.; Liu, W.; Qin, W.; Han, J.; Yang, K.; Luo, H.; Wang, D. Improvement for sulphidation roasting and its application to treat lead smelter slag and zinc recovery. *Can. Metall. Q.* **2014**, *54*, 92–100. [CrossRef]
26. Zhang, B.; Zhu, L.; Liu, W.; Han, J.; Jiao, F.; Qin, W. Sulfidization and Sulfur Fixation of Jarosite Residues During Reduction Roasting. *Metall. Mater. Trans. B* **2019**, *50*, 761–771. [CrossRef]
27. Liu, W.; Zhu, L.; Han, J.; Jiao, F.; Qin, W. Sulfidization mechanism of ZnO roasted with pyrite. *Sci. Rep.* **2018**, *8*, 1–12.
28. Han, J.; Liu, W.; Zhang, T.; Xue, K.; Li, W.; Jiao, F.; Qin, W. Mechanism study on the sulfidization of ZnO with sulfur and iron oxide at high temperature. *Sci. Rep.* **2017**, *7*, 1–12.
29. Li, M.; Peng, B.; Chai, L.; Peng, N.; Yan, H.; Hou, D. Recovery of iron from zinc leaching residue by selective reduction roasting with carbon. *J. Hazard. Mater.* **2012**, *237–238*, 323–330. [CrossRef]
30. Min, X.; Zhou, B.; Ke, Y.; Chai, L.; Xue, K.; Zhang, C.; Zhao, Z.; Shen, C. Sulfidization behavior of $ZnFe_2O_4$ roasted with pyrite: Sulfur inducing and sulfur-oxygen interface exchange mechanism. *Appl. Surf. Sci.* **2016**, *371*, 67–73. [CrossRef]
31. Wang, C.; Chen, L.; Zheng, Y.; Lv, J.; Huang, L.; Ji, C. Sulfidization Behaviour of Blast Furnace Dust at High Temperatures. *Russ. J. Non-Ferr. Metals* **2019**, *60*, 363–371. [CrossRef]
32. Zheng, Y.; Liu, W.; Qin, W.; Han, J.; Yang, K.; Luo, H. Selective reduction of $PbSO_4$ to PbS with carbon and flotation treatment of synthetic galena. *Physicochem. Probl. Miner. Process.* **2015**, *51*, 535–546.
33. Roy, S.; Nayak, D.; Rath, S. A review on the enrichment of iron values of low-grade Iron ore resources using reduction roasting-magnetic separation. *Powder Technol.* **2020**, *367*, 796–808. [CrossRef]
34. Wang, Y.; Yang, H.; Zhang, W.; Song, R.; Jiang, B. Study on recovery of lead, zinc, iron from jarosite residues and simultaneous sulfur fixation by direct reduction. *Physicochem. Probl. Miner. Process.* **2018**, *54*, 517–526.
35. Wang, Y.; Yang, H.; Jiang, B.; Song, R.; Zhang, W. Comprehensive recovery of lead, zinc, and iron from hazardous jarosite residues using direct reduction followed by magnetic separation. *Int. J. Miner. Metall. Mater.* **2018**, *25*, 123–130. [CrossRef]
36. Wang, Y.; Yang, H.; Hou, X.; Gao, W.; Gui, H.; Liu, Q. The effect of pellet technology on direct reduction of jarosite residues from zinc hydrometallurgy. *Physicochem. Probl. Miner. Process.* **2019**, *55*, 802–811.
37. Peng, N.; Peng, B.; Chai, L.; Liu, W.; Li, M.; Yuan, Y.; Yan, H.; Hou, D. Decomposition of zinc ferrite in zinc leaching residue by reduction roasting. *Procedia Environ. Sci.* **2012**, *16*, 705–714. [CrossRef]

38. Beauchemin, S.; Gamage McEvoy, J.; Thibault, Y.; MacKinnon, T. Partitioning of transition metals during magnetization of oxidized pyrrhotite tailings. *Miner. Eng.* **2020**, *156*, 106495. [CrossRef]
39. Yu, J.; Han, Y.; Gao, P.; Li, Y.; Yuan, S.; Li, W. An innovative methodology for recycling iron from magnetic preconcentrate of an iron ore tailing. *Physicochem. Probl. Miner. Process.* **2018**, *54*, 668–676.
40. Vinosha, P.; Mely, L.; Jeronsia, J.; Krishnan, S.; Das, S. Synthesis and properties of spinel $ZnFe_2O_4$ nanoparticles by facile co-precipitation route. *Optik* **2017**, *134*, 99–108. [CrossRef]
41. Roine, A. *HSC Chemistry®v 9 [Software]*; Outotec Research Oy Center: Pori, Finland, 2016.
42. Frost, R.; Weier, M.; Martens, W. Thermal decomposition of jarosites of potassium, sodium and lead. *J. Therm. Anal. Calorim.* **2005**, *82*, 115–118. [CrossRef]
43. Drouet, C.; Navrotsky, A. Synthesis, characterization, and thermochemistry of K-Na-H_3O jarosites. *Geochim. Cosmochim. Acta* **2003**, *67*, 2063–2076. [CrossRef]